Isolation, Synthesis, and Structure−Activity Relationship Study on Daphnane and Tigliane Diterpenes as HIV Latency-Reversing Agents

Ahmed H. H. El-Desoky,[†,‡,#] Keisuke Eguchi,[†,#] Naoki Kishimoto,[§] Toshifumi Asano,[⊥] Hikaru Kato,[†] Yuki Hitora,[†] Shunsuke Kotani,[⊥,▽] Teruya Nakamura,[○] Soken Tsuchiya,[‖] Teppei Kawahara,[▽] Masato Watanabe,[¶] Mikiyo Wada,[▽] Makoto Nakajima,[⊥] Takashi Watanabe,[□] Shogo Misumi,[§] Sachiko Tsukamoto[†,*]

[†] Department of Natural Medicines, Graduate School of Pharmaceutical Sciences, Kumamoto University, 5-1 Oe-honmachi, Kumamoto 862-0973, Japan

[‡] Pharmaceutical Industries Research Division, Pharmacognosy Department, National Research Centre, 33 El Bohouth St. (Former El Tahrir St.), Dokki, P.O. 12622, Giza, Egypt

[§] Department of Environmental and Molecular Health Sciences, Graduate School of Pharmaceutical Sciences, Kumamoto University, 5-1 Oe-honmachi, Kumamoto 862-0973, Japan

[⊥] Department of Organic Chemistry, Graduate School of Pharmaceutical Sciences, Kumamoto University, 5-1 Oe-honmachi, Kumamoto 862-0973, Japan

[▽] Department of Instrumental Analysis, Graduate School of Pharmaceutical Sciences, Kumamoto University, 5-1 Oe-honmachi, Kumamoto 862-0973, Japan

[○] Department of Structural Biology, Graduate School of Pharmaceutical Sciences, Kumamoto University, 5-1 Oe-honmachi, Kumamoto 862-0973, Japan

[‖] Department of Pharmaceutical Biochemistry, Graduate School of Pharmaceutical Sciences, Kumamoto University, 5-1 Oe-honmachi, Kumamoto 862-0973, Japan

¶ Technical Devision, Kumamoto University, 5-1 Oe-honmachi, Kumamoto 862-0973, Japan

 Department of Medicinal Botany, Graduate School of Pharmaceutical Sciences, Kumamoto University, 5-1 Oe-honmachi, Kumamoto 862-0973, Japan

# These authors contributed equally.

* Corresponding author.

E-mail address: sachiko@kumamoto-u.ac.jp (ST)

ABSTRACT: Three new diterpenes, stellejasmins A (**1**) and B (**2**) and 12-*O*-benzoylphorbol 13-heptanoate (**3**), were isolated from the root of *Stellera chamaejasme* L. The structures of **1**−**3** were elucidated by extensive NMR and mass spectroscopic analyses. Compounds **1** and **2** are the first derivatives containing a hydroxy group at C-2 in the family of daphnane and tigliane diterpenes. The presence of a chlorine atom in **1** is unique in the plant metabolite. Compound **3** has an odd-number acyl group, which is biosynthetically notable. HIV LTR-driven transcription activity was tested with **1**−**3** and 17 known diterpenes isolated from *S. chamaejasme* L. and *Wikstroemia retusa* A.Gray. Among these, gnidimacrin (**4**), stelleralide A (**5**), and wikstroelide A (**20**) were highly potent, with EC_{50} values of 0.14, 0.33, and 0.39 nM, respectively. The structure−activity relationship (SAR) was investigated using 20 natural and eight synthetic diterpenes. This is the first SAR study on natural daphnane and tigliane diterpenes.

INTRODUCTION

Acquired immunodeficiency syndrome (AIDS) is caused by human immunodeficiency virus (HIV), and 79.3 million people have been infected with HIV and 36.3 million people have died of AIDS according to the World Health Organization (WHO)[1]. At the end of 2019, 38 million people were affected by HIV, making AIDS a serious global health concern.

Although antiretroviral therapy (ART) suppresses virus replication, latent virus persists in viral reservoir cells and patients need to take ART treatment throughout life.[2−6] To eradicate HIV, the "shock and kill" approach is considered an effective strategy. In this strategy, the latent HIV reservoirs are activated by latency-reversing agents (LRA),[4,5] and LRA reverse viral latency and induce viral production in cells. The activated cells can be eliminated by apoptosis and immune-mediated clearance. Thus far, several natural compounds, including ingenol B, prostratin, phorbol 12-myristate 13-acetate, ingenol 3-angelate, and bryostatin, have been reported as potent LRA through alteration of protein kinase C (PKC).[7] Among these, the Wender group succeeded in synthesizing prostratin, originally isolated from *Pimelea prostrata* (Thymelaeaceae),[8] by five steps from phorbol,[9] a major constituent of croton oil in *Croton tiglium* (Euphorbiaceae). Furthermore, to achieve clinical applications with minimal side effects, they synthesized derivatives of prostratin, ingenol, and bryostatin as prodrugs of PKC modulators, and some of them exhibited more effective LRA activities.[10] On the other hand, Li, Chen, and Lee *et al.* reported that gnidimacrin (**4**), originally isolated from *Gnidia subcordata* (Thymelaeaceae) as an antileukemic daphnane diterpene,[11] eliminates latently HIV-infected cells at picomolar concentrations *ex vivo*.[12,13] In addition, they reported the structure−activity relationship (SAR) of anti-HIV replication activities of **4** and 29

synthetic derivatives, in addition to HIV latency activation activities of **4** and three selected derivatives.[14] Recently, Li, Wu, and Zhang *et al.* isolated a tigliane and 10 daphnane diterpenes from the buds of *Wikstroemia chamaedaphne* (Thymelaeaceae), and among them wikstroelide E (**7**), originally isolated from *W. retusa* as an antileukemic diterpene,[15,16] demonstrated 2500-fold more potent latency-reversing activity than prostratin.[17] Furthermore, Siani *et al.* reported that 4-deoxy-4*β*-phorbol-12-tiglate-13-phenylacetate, isolated from the latex of *Euphorbia umbellate* (Euphorbiaceae), is effective in reactivating 62.1% of the virus latency at 0.091 nM.[18] To develop new clinically available LRA from structurally-diverse natural products, we performed bioassay-guided purification of the extract of *Stellera chamaejasme* L. (Thymelaeaceae) and *W. retusa* A.Gray, and examined the SAR of HIV LTR-driven transcription activities with 20 daphnane/tigliane diterpenes (**1**−**20**), including three new compounds **1**−**3**, and eight synthetic derivatives **21**−**28**.

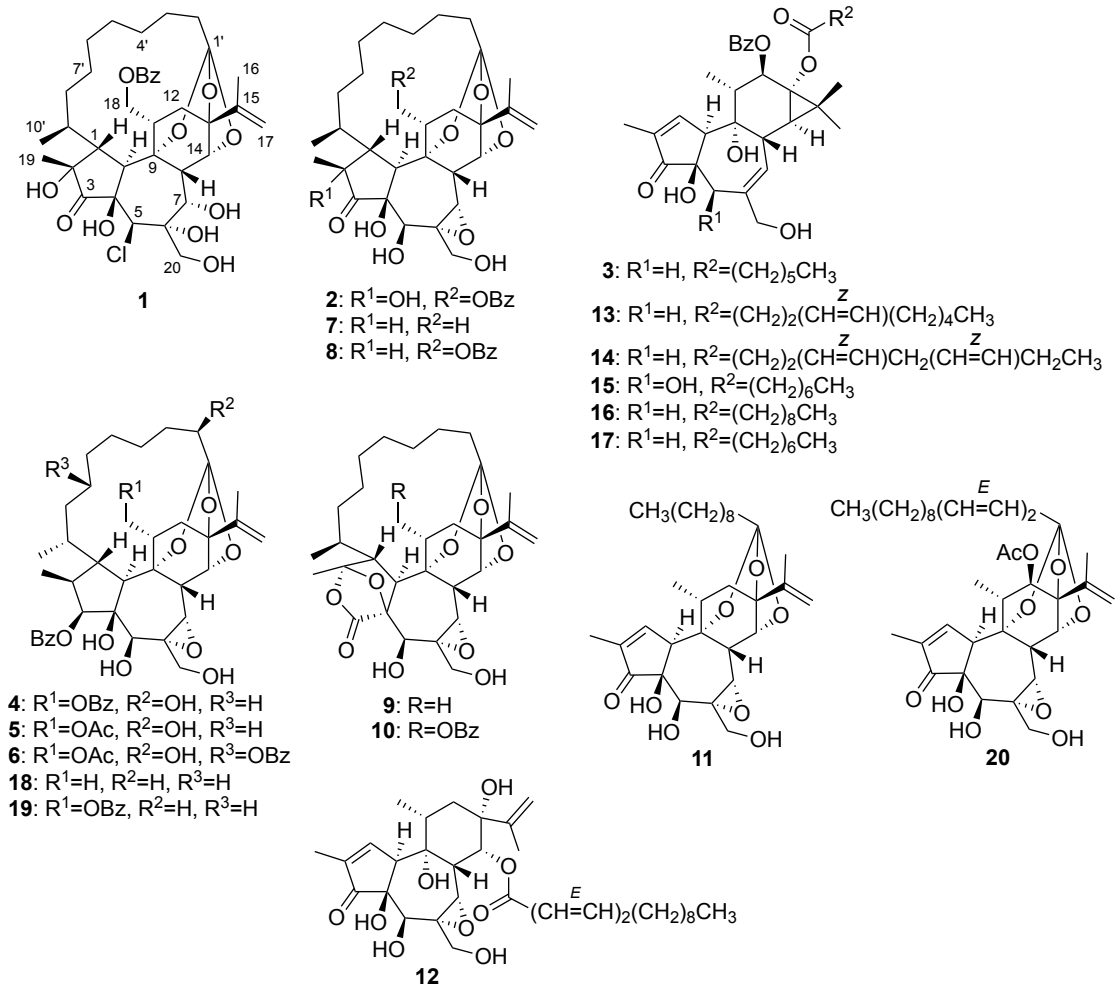

Figure 1. Structures of compounds **1**–**20**.

RESULTS

Isolation and Structures of Compounds with HIV LTR-driven Transcription Activities from *S. chamaejasme* and *W. retusa*. Root of *S. chamaejasme* was collected in Nepal and extracted with MeOH. The extract was subjected to bioassay-guided isolation to afford two new daphnane diterpenes with macrocyclic rings, stellejasmins A (**1**) and B (**2**), and a new tigliane diterpene, 12-*O*-benzoylphorbol 13-heptanoate (**3**), along with 14 known diterpenes, gnidimacrin[11] (**4**), stelleralide A[19] (**5**), stelleralide F[20]

(**6**), wikstroelides E and F[15] (**7** and **8**), pimelotide A[21] (**9**), stelleralide C[19] (**10**), simplexin[22,23] (**11**), wikstroelide M[16] (**12**), stelleracins A−C[24] (**13**−**15**), stellerarin[25] (**16**), and 12-*O*-benzoylphorbol 13-octanoate[26–28] (**17**) (Figure 1). Stem bark of *W. retusa* collected in Ishigaki-island (Japan) was extracted with MeOH, and the extract was purified to afford six known diterpenes, **7**, **9**, **13**, pimelea factor P2[29] (**18**), stelleralide B[19] (**19**), and wikstroelide A[15] (**20**).

The ^{1}H and ^{13}C NMR spectra of **1** and **2** in $CDCl_3$ (Tables S1 and S2) displayed characteristic signals reminiscent of alkyldaphnane diterpene. The NMR spectra of **2** (Figure S17) were superimposable on those of **8** (Figure S39) except for the presence of a hydroxy [δ_C 79.6 (C-2)] and a singlet methyl [δ_H 1.37 (s, H_3-19) and δ_C 21.0 (C-19)] groups in **2** instead of a methine (C-2), and doublet methyl (C-19) groups in **8**. These were supported by HMBCs from H_3-19 to C-1, C-2, and C-3 and from H-9', H-1, and H-10 to C-2 (Figure 2a), indicating that a hydrogen at C-2 in **8** is replaced with a hydroxy group in **2**. This planar structure is supported by the molecular formula of **2**, $C_{37}H_{48}O_{11}$, shown by HRTOFMS. In the NOESY spectrum of **2**, correlations of H-8'/H_3-19, H-1/H_3-19, and H-1/H-18b revealed that these protons are β-orientated, whereas correlations of H-10/H_3-10', H-5/H-10', and H-5/H-10 indicated their α-orientations (Figure 2a). This demonstrated that the hydroxy group at C-2 is α-orientated and the relative configuration of **2** is the same as those of **7** and **8**.[15,30] Wikstroelides E (**7**) and F (**8**) were originally isolated from *W. retusa* and reported to have 9'*R*-configurations.[15] After that, 1,2-dihydro-5-hydroxy-9'-methyl-6a,7a-epoxy-12b-acetoxy-9,13,14-ortho-1a-decenoate-resiniferonol-10'-oic acid was isolated as a mixture of C9'-epimers (*R*:*S*, 4:6) from *P. elongate* along with **7**.[30] In the paper, C9'-configurations of the respective epimers were determined by ROESY spectrum, and by the comparison of their ^{13}C chemical shifts, C-

9' of **7** was changed to be *S*.[30] Accordingly, C-9' of **8** also should be changed to *S*. The absolute configuration of **2** was determined by comparing the ECD spectrum with **8** (Figure 2b). The ECD pattern with positive and negative Cotton effects of **2** matched that of **8**, exhibiting the same absolute configuration.

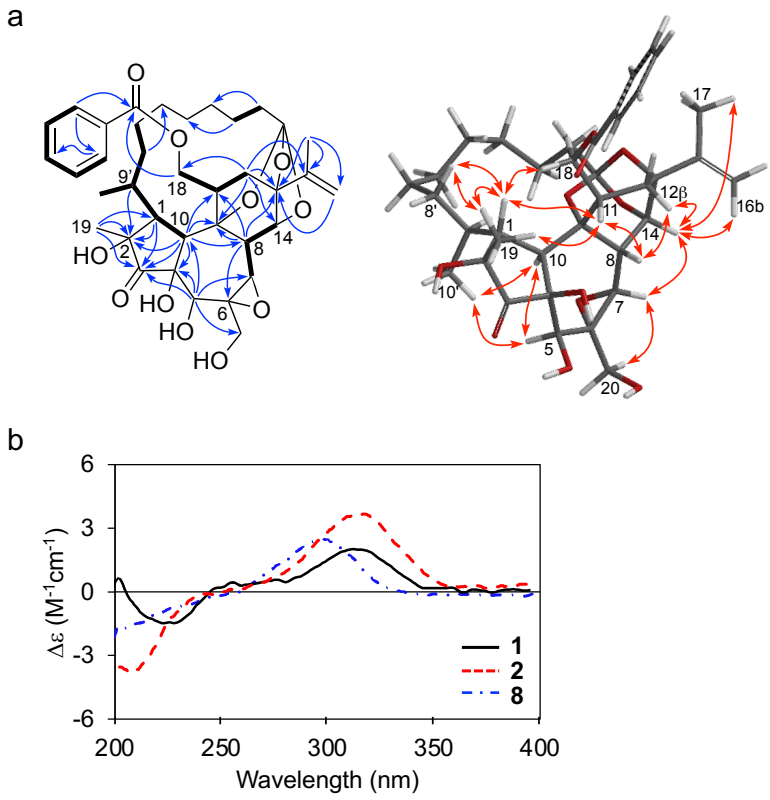

Figure 2. a) COSY correlations (bold lines), HMBCs (blue arrows), and NOE correlations (red arrows) of **2**. b) ECD spectra of **1**, **2**, and **8**.

The molecular formula of **1** was demonstrated to be $C_{37}H_{49}ClO_{11}$ by HRTOFMS, indicating the presence of a chlorine atom by isotopic peaks at *m/z* 705/707, with an intensity of 3:1. On comparison of the NMR spectra of **1** and **2**, large differences were observed for H_2-20 (**1**: δ_H 3.96/4.09, **2**: δ_H 3.80/3.86), C-20 (**1**: δ_C 69.6, **2**: δ_C 65.3), C-6

(**1**: δ_C 76.5, **2**: δ_C 60.8), and C-7 (**1**: δ_C 82.1, **2**: δ_C 64.1). This along with the molecular formula suggest that the 6,7-epoxide of **2** was cleaved into two hydroxyls in **1**. Among 11 oxygens in **1**, six were assigned to the orthoester function, the ester function at C-18, and the ketonic carbonyl C-3, which was inferred by the corresponding chemical shifts of **2**. The remaining five oxygens and a chlorine in **1** were attached to the remaining six carbons, C-2 (δ_C 79.2), C-4 (δ_C 77.7), C-5 (δ_C 71.7), C-6 (δ_C 76.5), C-7 (δ_C 82.1), and C-20 (δ_C 69.6). To determine the positions of oxygens, the HMBC spectrum was measured in pyridine-d_5 (Table S3). The presence of hydroxyl groups was revealed to be C-4 and C-7 by HMBC correlations, from 4-OH [δ_H 6.56 (s)] to C-3 (δ_C 213.4), C-4 (δ_C 81.1), and C-10 (δ_C 45.3), and from 7-OH [δ_H 6.08 (s)] to C-6 (δ_C 83.3), C-7 (δ_C 77.3), and C-8 (δ_C 37.4), together with a COSY correlation of 7-OH/H-7 [δ_H 5.40 (s)] (Figure 3a). Next, the ^{13}C chemical shifts measured in CD_3OD and CD_3OH were compared (Figure 3b and Table S4), and large deshielded shifts (δ in CD_3OD − δ in CD_3OH) were observed for C-2 (−0.089), C-4 (−0.144), C-6 (−0.176), C-7 (−0.150), and C-20 (−0.074) compared with C-5 (−0.023), which confirmed that the chlorine is attached to C-5. NOE correlations of H-8/H-20 and H-7/H-14 demonstrated α-orientations of 6-OH and 7-OH, and correlations H-10/H_3-10', H-5/H_3-10', and H-5/H-10 suggested that the chlorine atom is β-orientated (Figure 3a). The ECD pattern of **1** was similar to those of **2** and **8**, indicating the same absolute configurations (Figure 2b).

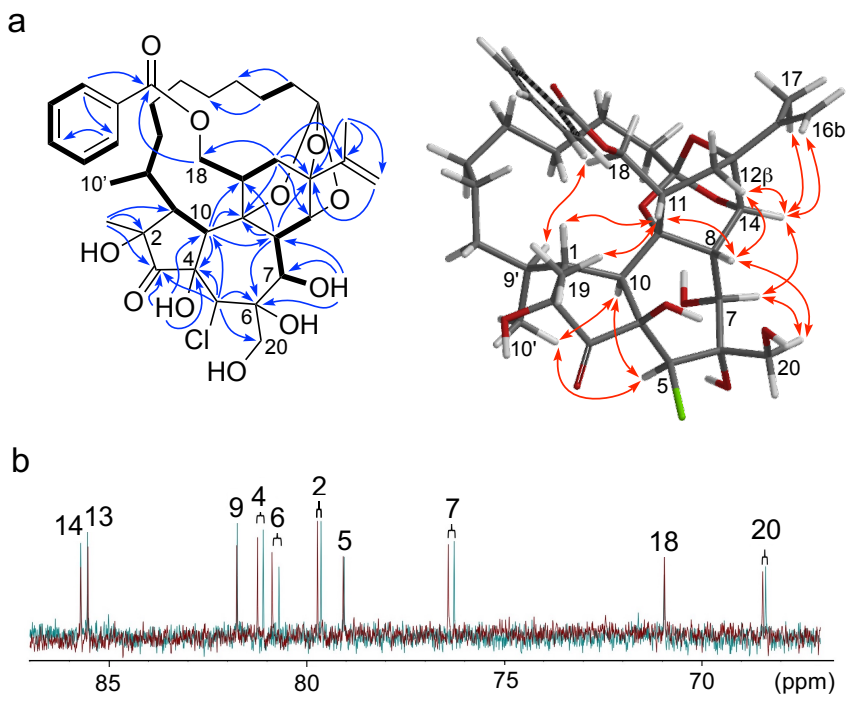

Figure 3. a) COSY correlations (bold lines), HMBCs (blue arrows), and NOE correlations (red arrows) of **1**. b) ^{13}C NMR spectra in CD_3OD (green) and CD_3OH (red) of **1**.

Compound **3** exhibited a sodiated molecular ion peak at *m/z* 603.2925 $[M + Na]^+$ by HRTOFMS corresponding to the molecular formula $C_{34}H_{44}O_8$. The ^1H and ^{13}C NMR spectra (Table S5) of **3** were almost superimposable on those of 12-*O*-benzoylphorbol-13-octanoate (**17**) (Table S39). The ^{13}C NMR spectrum and molecular formula revealed the presence of a heptanoyl group at C-13 in **3**, which was supported by a spin system H_2-2"/H_2-3"/H_2-4"/H_2-5"/H_2-6"/H_2-7" observed in the TOCSY spectrum and the HMBCs from two methylenes H_2-2" and H_2-3" to a carbonyl carbon C-1" (Figure 4). This suggested that the structure of **3** is attributed to 12-*O*-benzoylphorbol 13-heptanoate. The NOE correlations (Figure 4) had the same relative configuration as **17**, and the specific

rotation of **3** [+14 (*c* 0.70, MeOH)] indicated the same absolute configurations as **17** [+2.1 (*c* 2.1, MeOH); lit.[26] +8.1695 (*c* 0.590, MeOH)] and 12-*O*-benzoylphorbol 13-nonanoate [lit.[27] +7 (*c* 0.09, MeOH)].

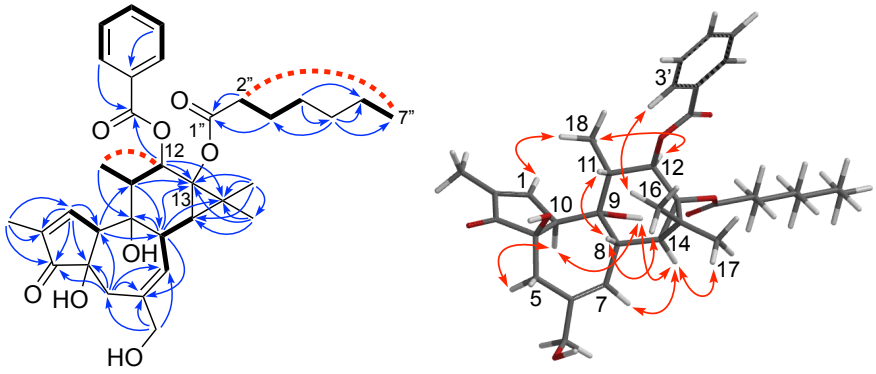

Figure 4. COSY (bold lines) and TOCSY (red dashed bold lines) correlations, HMBCs (blue arrows), and NOE correlations of **3**.

SAR Study on LTR-driven Transcription Activities of 1−28. LTR-driven transcription activities in HIV were tested with natural (**1**−**20**) (Figure 5) and synthetic (**21**−**28**) (Scheme 1, Table 1) diterpenes. Among these, **4** was the most potent, with an EC_{50} value of 0.14 nM, and **5** and **20** were effective (0.33 and 0.39 nM, respectively). (1) First, daphnane diterpenoids, having a macrocyclic bridge between the aliphatic orthoester group and the C-1 position, were tested. (1-1) Compounds **2**, **4**, **8**, and **10** had structural differences in the five-membered rings (Figure 5a). Compound **4**, with a benzoyloxy group at C-3, was the most potent and **8**, comprising a ketone at C-3, was the second. Compounds with a hydroxy group at C-2 (**2**) and with an oxygen bridged-lactone (**10**) significantly reduced the activity. Similarly, **1** and **9** had weaker activity (Figure 5a). Therefore, the structure of the five-membered ring in daphnane diterpenoids is important

for the LTR-driven transcription activity, and the substituents at C-2 and C-3 are essential (Figure 6a). (1-2) Compounds **5**, **6**, **18**, and **19** are variations of the most potent compound **4**, and the substituents at C-18 hardly affected the activities (**4** versus **5**; **18** versus **19**) (Figure 5b). The absence of the hydroxy group at C-2' reduced the activity (**4** > **19**). The presence of the benzoyloxy group at C-7' reduced the activity (**5** > **6**). As with **18** and **19**, **7** and **8** were nearly equipotent (Figures 5b, 6a). (2) Next, LTR-driven transcription activities of tigliane diterpenoids were compared. (2-1) The diterpenoids isolated from *S. chamaejasme* and *W. retusa* possess benzoyloxy and alkyloxy groups at C-12 and C-13, respectively. Although the alkyl chains differ in length, the activities of **3**, **16**, and **17** were almost equipotent (Figure 5c). Of note, the presence of a hydroxy group at C-5 reduced the activity (**17** > **15**) (Figure 5c), suggesting that this hydroxy group slightly hampers the interaction in the binding site of human PKCβ (Figure 6b). (2-2) Compounds **13**, **14**, and **16** contain C_{10}-acyl groups, and **13** and **14** have 4*Z* and 4*Z*,7*Z* double bonds, respectively. They were equipotent and the saturated alkyl chain (**16**) increased the activity (Figure 5d). In contrast, a daphnane diterpene **20** having a (1*E*,3*E*)-dienyl moiety was more potent than **11** with a saturated alkyl chain (Figure 5d). (3) The isolated amount of **13** was limited (0.57 mg), and **13** was synthesized from a commercially available phorbol (Scheme 1). After tritylation of the primary hydroxy group (C-20) with trityl chloride, an acylation sequence of hydroxy groups at C-12 and C-13 with benzoyl and (4*Z*)-decenoyl groups consequently produced an unfavorable diester **21**. This suggested that the C-12 hydroxy group is sterically more hindered by a methyl group (C-18) and is less reactive, which predominantly promoted the first benzoylation of even tertiary hydroxy group at C-13. We revised the acylation sequence to obtain 13-*O*-4*Z*-decenoylated and then 12-*O*-benzoylated diester **13**. The natural and synthetic **13** were

equipotent with EC_{50} values of 4.2 and 5.8 nM, respectively (Figure 5d, Table 1). As **13** is slightly more potent than **21** (Table 1), the positions of the substituents at C-12 and C-13 are important. To assess the effects of the geometry of the double bond, 13-*O*-4*E*-decenoyl derivative **23** was prepared, demonstrating that the geometry tolerates the efficacy (**13** versus **23**) (Table 1, Figure 6b). Although the activities of **3**, **16**, and **17** were equipotent (Figure 5c), the propionate (**22**) and stearate (**24**) derivatives were less potent (Table 1) than these three compounds, suggesting that the potency requires a suitable acyl chain length (Figure 6b). To evaluate the effects of the double bonds, derivatives **24**−**28** with 13-*O*-C_{18}-acyl groups, were synthesized (Table 1). Although **24** with a saturated fatty acid was less active, **25**−**28** with one to three double bonds improved the efficacy, revealing that the number and position of double bonds are not important for the effects (Figure 6b).

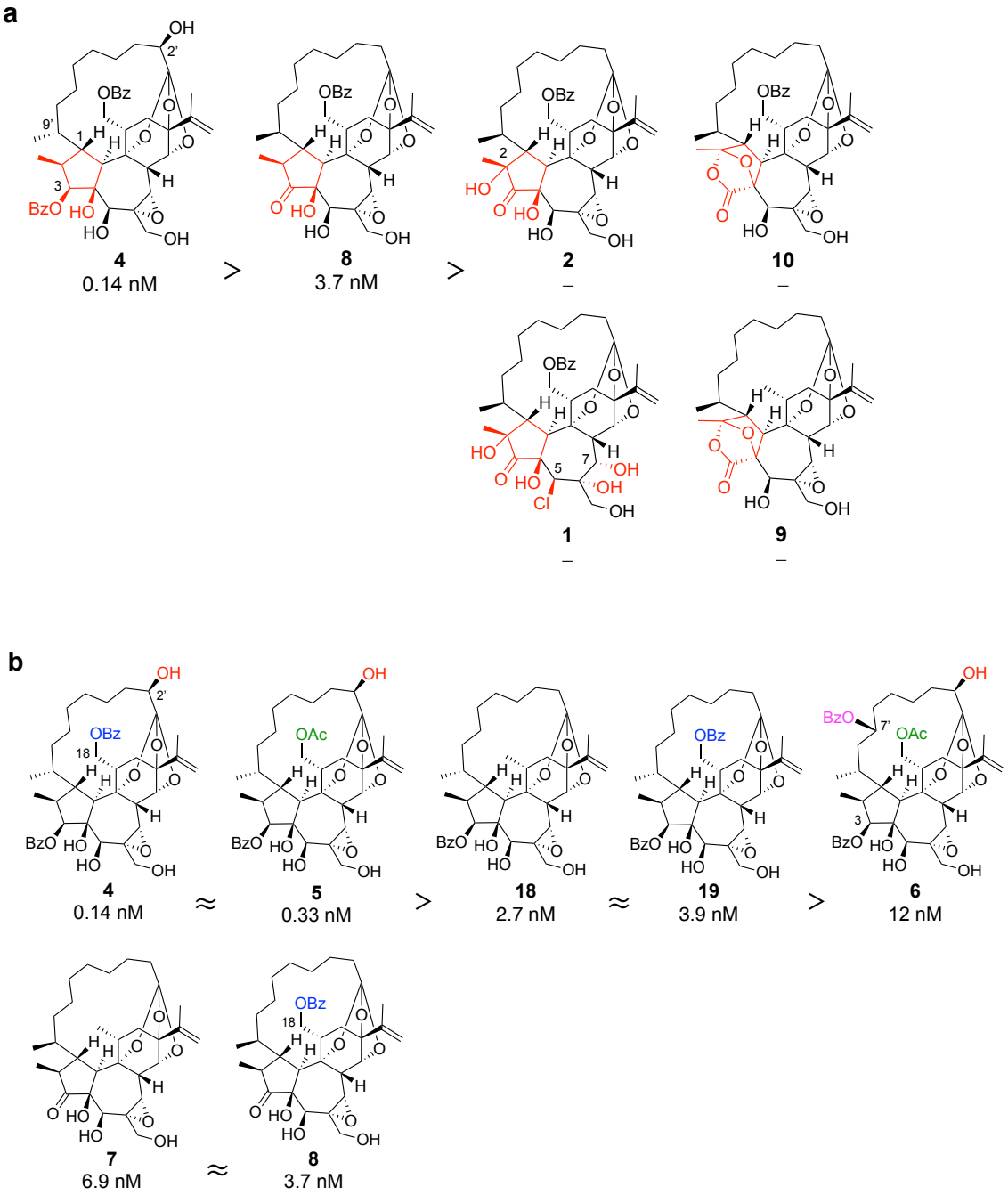

Figure 5. Comparison of the structures of **1**−**11** and **13**−**20** and their EC_{50} values of LTR-driven transcription activities (**a**−**d**). The activities are shown under the compound numbers. EC_{50} values were calculated for the compounds, which were more than two-times greater than the relative value of DMSO. The activities of **1**, **2**, **9**, **10**, and **12** were less than this index.

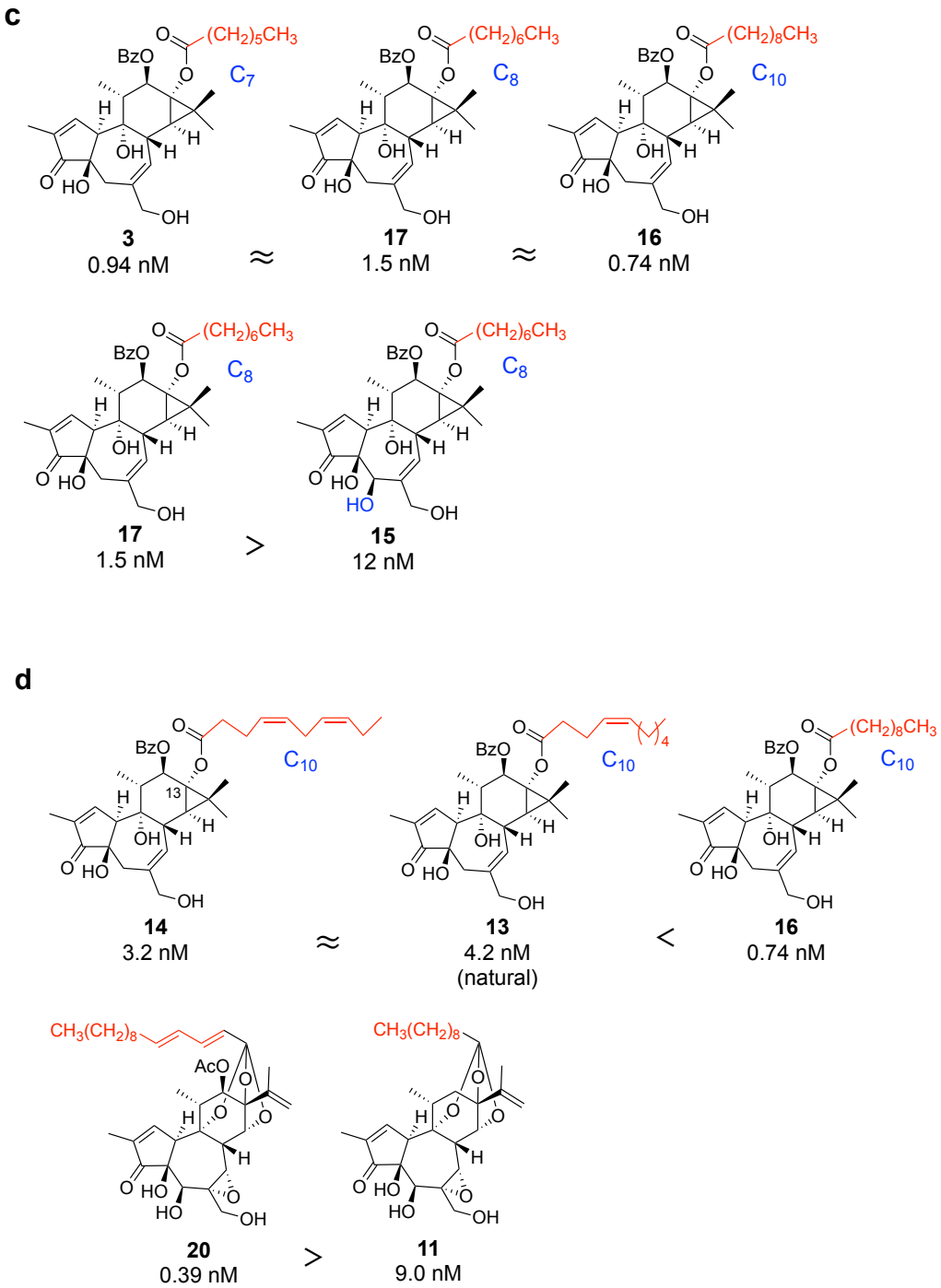

Figure 5. Continued.

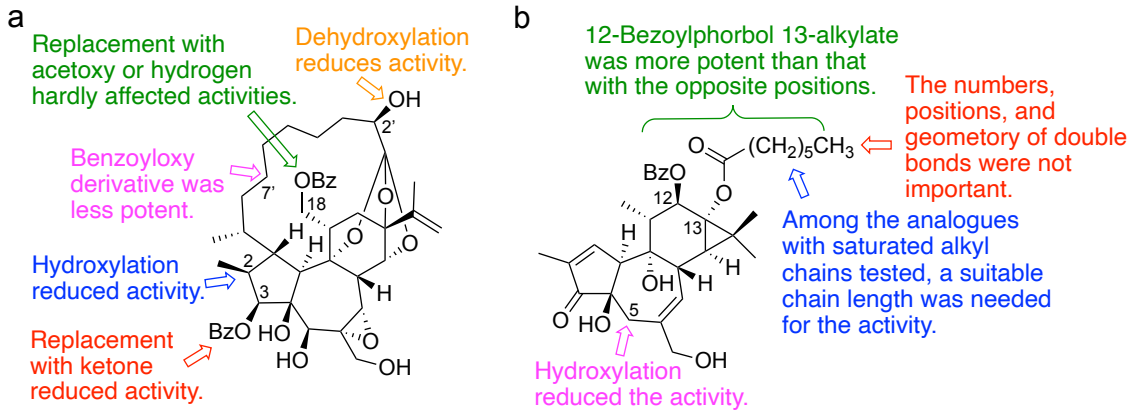

Figure 6. Summary of the SAR of LTR-driven transcription activities of daphnane (a) and tigliane (b) diterpenes.

Scheme 1. Syntheses of 13 and 21 from Phorbol [a]

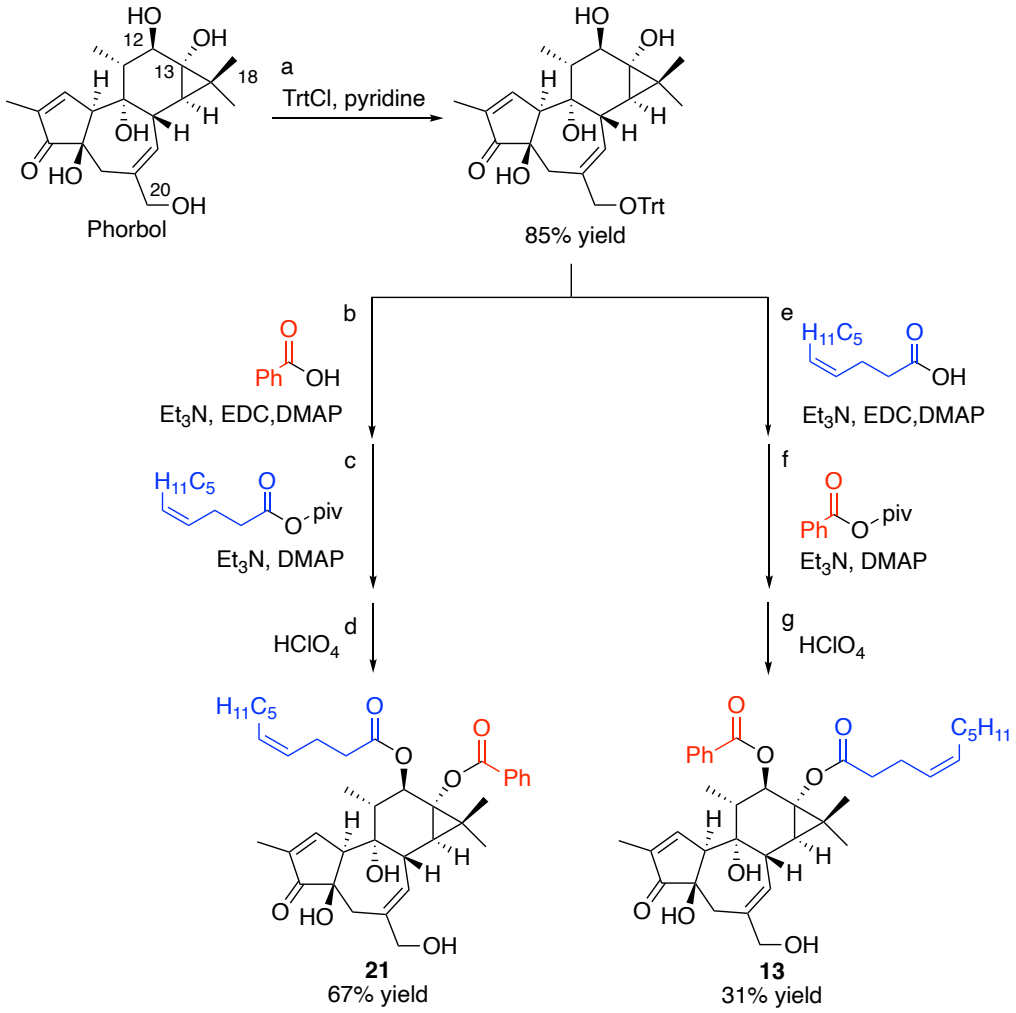

[a] Reagents and conditions: (a) Trytyl chloride, pyridine, rt, 19 h, in the dark; (b) benzoic acid (1.1 eq), Et_3N (2.0 eq), EDC (1.3 eq), DMAP (20 mol %), CH_2Cl_2, rt, 72 h, in the dark; (c) (4*Z*)-decenoic pivalic anhydride (6.0 eq), Et_3N (7.0 eq), DMAP (4.0 eq), CH_2Cl_2, rt, 15 h, in the dark; (d) $HClO_4$ (2.0 eq), MeOH, rt, 1 h, in the dark; (e) (4*Z*)-decenoic acid, (1.1 eq), Et_3N (2.0 eq), EDC (1.3 eq), DMAP (20 mol %), CH_2Cl_2, rt, 72 h, in the dark; (f) benzoic pivalic anhydride (6.0 eq), Et_3N (7.0 eq), DMAP (4.0 eq), CH_2Cl_2, rt, 15 h, in the dark; (g) $HClO_4$ (2.0 eq), MeOH, rt, 1 h, in the dark.

Table 1. LTR-driven Transcription Activity of Synthetic Diterpenes 21−28 and 13 against HIV [a]

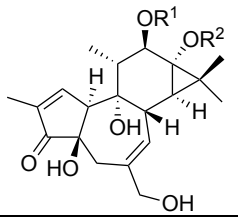

cmpd	R^1	R^2	EC_{50} (nM)
21	$CO(CH_2)_2(CH^{Z}{=}CH)(CH_2)_4CH_3$	Bz	18
22	Bz	$COCH_2CH_3$	10
23	Bz	$CO(CH_2)_2(CH^{E}{=}CH)(CH_2)_4CH_3$	5.8
24	Bz	$CO(CH_2)_{17}CH_3$	– [b]
25	Bz	$CO(CH_2)_7(CH^{Z}{=}CH)(CH_2)_7CH_3$	16
26	Bz	$CO(CH_2)_7(CH^{Z}{=}CH)CH_2(CH^{Z}{=}CH)(CH_2)_4CH_3$	13
27	Bz	$CO(CH_2)_7(CH^{Z}{=}CH)CH_2(CH^{Z}{=}CH)CH_2(CH^{Z}{=}CH)CH_2CH_3$	7.6
28	Bz	$CO(CH_2)_4(CH^{Z}{=}CH)CH_2(CH^{Z}{=}CH)CH_2(CH^{Z}{=}CH)(CH_2)_4CH_3$	10
13	Bz	$CO(CH_2)_2(CH^{Z}{=}CH)(CH_2)_4CH_3$	5.6

[a] Compounds tested exhibited no cytotoxicity up to 0.1 μM in TZM-bl cells.

[b] EC_{50} values were calculated for the compounds, which were more than two-times greater than that of the relative value of DMSO.

Molecular Docking Simulations. Molecular docking simulations of four compounds **2**, **4**, **8**, and **10** were performed using the Molecular Operating Environment (MOE version 2020.09) (See Experimental Section). As phorbol 13-acetate binds to mouse PKCδ with C-3 ketone, C-4 hydroxyl, and C-20 hydroxyl groups,[31] the simplified models **2a**, **4a**, **8a**, and **10a** (Figure 7a) were used for docking at the ligand-binding site of the modeled human PKCβ structure generated from the structure of mouse PKCδ in complex with phorbol 13-acetate (PDB ID: 1PTR) (Figures S85a, b).[31] The molecular docking simulations revealed five binding modes for each compound and ranked them by docking scores (GBVI/WSA dG scores).[32] Each binding mode with significantly best scores of **4a**, **8a**, and **10a** (-7.1, -6.4, and -6.1 kcal/mol, respectively) was similar to that of phorbol 13-acetate (Figures 7b, c, 8). On the other hand, the molecular docking simulation of **2a** showed various binding modes with scores of approximately -6 kcal/mol and no specific binding mode with a significantly best score was found. Thus, the binding mode of **2a** with -6.0 kcal/mol (Figures 7b, 8), which is similar to that of phorbol 13-acetate, was used for the following discussion. Model **4a** had the best docking score (-7.1 kcal/mol) compared with the other simplified models. In the binding mode of **4a**, the benzoyl group at C-3 makes van der Waals contacts and a hydrogen-bond with human PKCβ. The phenyl ring interacts with Cα-H of Gly124 and the carbonyl oxygen forms a hydrogen-bond with the main chain N-H of Gly124. These interactions play a role in the highest binding affinity of **4a** among the simplified models. Model **8a** had the second-best docking score (-6.4 kcal/mol) and its binding mode was similar to that of **4a** except for the interactions of the C-3 substituents (Figures 8a, b). On the other hand, the docking scores of **10a** and **2a** were -6.1 and -6.0 kcal/mol, respectively, suggesting the lower binding affinity of **10a** and **2a**. In the binding modes of **10a** and **2a**, the structurally different parts shown in red

(Figure 7a) are away from the binding surface of human PKCβ compared with those of **4a** and **8a** (a black arrow in Figure 8a), indicating the lower binding affinity of **10a** and **2a**. The carbon framework of **2a** is identical to that of **8a** except for the presence of the hydroxy group at C-2 (Figure 7a). Although structurally similar, the binding modes of **8a** and **2a** are different (Figure 8a), which may be caused by the presence of the C-2 hydroxy group. The resulting docking scores of four simplified models are consistent with LTR-driven transcription activities of their original structures (Figure 7b). Compounds **4** and **8** with significant potencies (EC_{50}, 0.14 and 3.7 nM, respectively) had good docking scores for their simplified models **4a** and **8a** (-7.1 and -6.4 kcal/mol, respectively), whereas **10** and **2** with low potencies had insignificant scores for **10a** and **2a** (-6.1 and -6.0 kcal/mol, respectively).

a

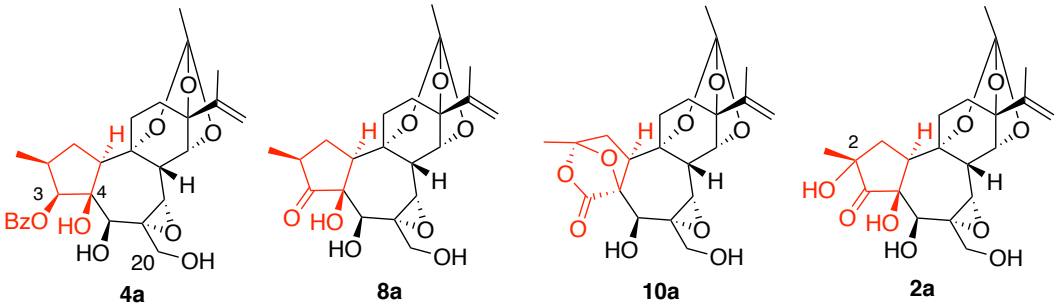
4a
8a
10a
2a

b

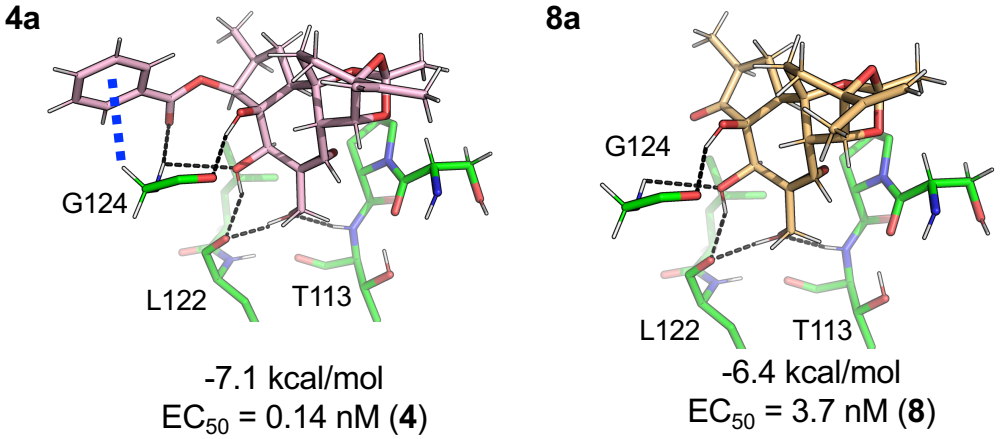
4a
G124
L122
T113
-7.1 kcal/mol
EC50 = 0.14 nM (4)
8a
G124
L122
T113
-6.4 kcal/mol
EC50 = 3.7 nM (8)
10a
G124
L122
T113
-6.1 kcal/mol
EC50 = NA (10)
2a
G124
S111
L122
T113
-6.0 kcal/mol
EC50 = NA (2)

c

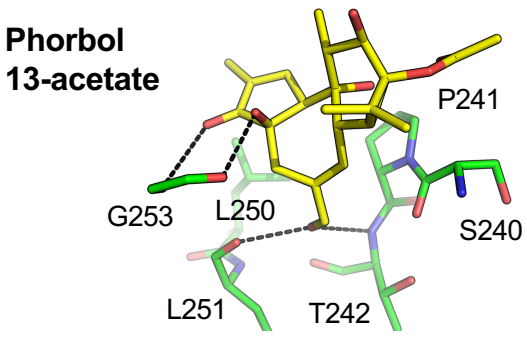
Phorbol
13-acetate
P241
G253
L250
S240
L251
T242

Figure 7. (a) Structures of the simplified models **4a**, **8a**, **10a**, and **2a**. The structurally different parts are shown in red. (b) Binding modes of the simplified models **4a**, **8a**, **10a**, and **2a**. The binding modes of **4a**, **8a**, **10a**, and **2a** in the ligand-binding site of the modeled human PKC*β* are shown as stick representations. Hydrogen bonds are shown as black dashed lines. Van der Waals contacts are shown as a thick blue dashed line. The docking scores of **4a**, **8a**, **10a**, and **2a** (GBVI/WSA dG scores), and the EC_{50} values of **4**, **8**, **10**, and **2** are indicated below the structures. (c) The binding mode of phorbol 13-acetate in mouse PKC*δ* (PDB ID: 1PTR).

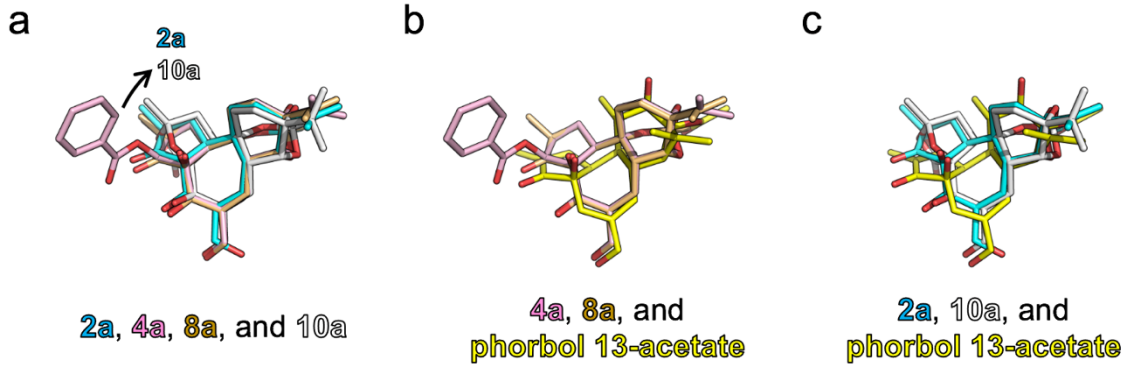

Figure 8. Comparison of the binding modes. (a) All the simplified models (**2a**, cyan; **4a**, pink; **8a**, brown; **10a**, white). A black arrow indicates that **2a** and **10a** are away from the binding surface of human PKC*β* compared with **4a** and **8a**. (b) Models **4a** and **8a** and phorbol 13-acetate (yellow). The structure of phorbol 13-acetate is shown by superposition of the mouse PKC*δ*/phorbol 13-acetate complex onto the modeled human PKC*β*. (c) Models **2a** and **10a** and phorbol 13-acetate.

DISCUSSION AND CONCLUSIONS

Fatty acids are biosynthesized from acetyl-CoA and composed of even carbon numbers. Therefore, natural products having odd-carbon-chain fatty acids are highly unique. Thus far, as diterpenes having odd-carbon-chain fatty acids, 12-*O*-benzoylphorbol 13-

nonanoate[27] and wikstroelides C[15] and N,[16] containing *trans*-5-pentadecenoyl group, were isolated from *Daphne aurantiaca* and *W. retusa*, respectively. These plants and *S. chamaejasme*, belonging to the family Thymelaceae, may have the biosynthetic pathway to produce odd-carbon-chain fatty acids. Isolation of chlorinated natural products from plants is also uncommon. Although ten chlorinated daphnane diterpenoid orthoesters were isolated from *Trigonostemon cherrieri* (Euphorbiaceae),[33,34] chlorine attaches at C-9 in all compounds. Compound **1** is the first example that possesses a chlorine atom at a position other than C-9. Chlorinated secondary metabolites in plants are novel, and the plants in the families Euphorbiaceae and Thymelaceae may have the enzymes for chlorination.

Although the SAR study on anti-HIV replication activities of 29 synthetic gnidimacrin derivatives was reported,[14] this is the first SAR study on LTR-driven transcription activities of natural daphnane/tiglian diterpenes (Figure 6). In our study, the relationship between the five-membered ring of daphnane diterpenes (**4** > **8** > **10** and **2**) and the LTR-driven transcription activities are the most notable (Figure 5a). The previous study reported that oxygen atoms at C-3, C-4, and C-20 of phorbol 13-acetate form a hydrogen-bond network with the conserved amino acid residues, Thr242, Leu251, and Gly253 of mouse PKCδ.[31] As with phorbol 13-acetate, the simplified models (**4a**, **8a**, **10a**, and **2a**) showed six, five, four, and five hydrogen-bond interactions in the binding site of the human PKCβ, respectively, and their docking scores are consistent with the LTR-driven transcription activities (Figure 7b). The previous studies[35,36] revealed that the long-chains at C-12 and C-13 esters play an important role to translocate the phorbol ester-bound PKC to the membrane to activate PKC, followed by LRA activity. We demonstrated that the potency requires a suitable saturated aliphatic chain length (**3**, **16**,

and **17** versus **22** and **24**) (Figure 5c, Table 1). Regarding the effects of unsaturated aliphatic chains, the LTR-driven transcription activities of compounds with C_{10}-acyl groups (**13**, **14**, and **16**) (Figure 5d) and C_{18}-acyl groups (**24**−**28**) (Table 1) had different efficacies. Of the compounds with C_{10}-acyl groups, those with unsaturated aliphatic chains (**13** and **14**) are less potent than that with the saturated chain (**16**), and of the compounds with C_{18}-acyl groups, those with unsaturated aliphatic chains (**25**−**28**) are more potent than that with the saturated chain (**24**). The effects of the double bonds on the LTR-driven transcription activities are different for C_{10}- and C_{18}-acyl groups. Although it remains unclear, the SAR study may aid in developing effective LRA for clinical use. Our laboratories are currently conducting *in vivo* studies of LRA using candidates.

EXPERIMENTAL SECTION

General Experimental Procedures. Optical rotations were measured on a JASCO DIP-1000 polarimeter in MeOH, UV spectra on a JASCO V-550 spectrophotometer in CH_3CN, and ECD spectra on a JASCO J-820 spectropolarimeter in CH_3CN. IR spectra were recorded on a PerkinElmer Frontier FT-IR spectrophotometer. ^1H and ^{13}C NMR spectra were recorded on a Bruker Avance III 600 NMR spectrometer or Bruker Avance III 500 NMR spectrometer in $CDCl_3$, CD_3OD, CD_3OH, or pyridine-d_5. Chemical shifts were referenced to the residual solvent peaks (δ_H 7.24 and δ_C 77.0 for $CDCl_3$; δ_H 3.31 and δ_C 49.0 for CD_3OD and CD_3OH; δ_H 7.55 and δ_C 135.5 for pyridine-d_5). HRTOFMS spectra were measured on a Waters Xevo G2-XS Qtof mass spectrometer. LC-MS experiments were performed on a Shimadzu LC-20AD solvent delivery system with a Shimadzu SPD-M20A photodiode array detector, which was interfaced to a Bruker

amaZon Speed mass spectrometer. The preparative MPLC was performed on a Biotage Isolera I. The preparative HPLC system comprised a Waters 515 HPLC pump and Waters 2489 UV/visible detector. The purities of the compounds are > 95%, which were confirmed by ^{1}H NMR spectra and LC-MS.

Plant Material. Root of *Stellera chamaejasme* L. (Thymelaeaceae) was collected by one of the authors (T.W.) from Nepal in July 2002 and identified by Dr. Takahide Kurosawa (Faculty of Symbiotic System Science, Fukushima University). A voucher specimen (no. LOM-SP020729(047)) was deposited in the herbarium of the University of Tokyo. Bark of *Wikstroemia retusa* A.Gray (Thymelaeaceae) was collected from Hirakubo Peninsula on Ishigaki Island (Japan) in September 2020. The plant was identified by one of the authors (M.W.). A voucher specimen (no. KUM-20200928-1) was deposited in the Faculty of Life Sciences, Kumamoto University.

Extraction and Isolation. Root of *S. chamaejasme* (2 kg) was extracted with MeOH. The MeOH extract (219 g) was concentrated under a vacuum and its suspension in water was extracted with EtOAc. The EtOAc-soluble fraction (125 g) was partitioned between *n*-hexane and 90% MeOH−H_2O. The 90% MeOH−H_2O soluble fraction (109 g) was subjected to SiO_2 column chromatography with stepwise gradient elution using CH_2Cl_2, 90, 85, and 80% CH_2Cl_2−MeOH, and CH_2Cl_2−MeOH−H_2O (6:4:1) to give fifteen fractions (A1−A15). Fraction A5 (13.2 g) eluted with 90% CH_2Cl_2−MeOH was subjected to ODS column chromatography with 40, 60, 80, 90, and 100% MeOH−H_2O to give 13 fractions (B1−B13). Fraction B11 (724 mg) was purified by HPLC (COSMOSIL 5C_{18}-MS-II, 20 × 250 mm, Nacalai Tesque Inc.) with 80% MeOH−H_2O to yield 18 fractions (C1−C18). Fraction C14 was identified as **4** (32.5 mg). Fraction C6 (6.4 mg) was purified by HPLC (COSMOSIL 5C_{18}-MS-II, 20 × 250 mm) with 70% MeCN−H_2O to yield **17**

(2.76 mg). Fraction C12 (29.2 mg) was purified by HPLC (InertSustain Phenylhexyl, 20 × 250 mm, GL Sciences Inc.) with 80% MeOH−H_2O to yield **13** (0.57 mg) and **7** (0.45 mg). Fraction C13 (9.8 mg) was purified by HPLC (InertSustain Phenylhexyl, 20 × 250 mm) with 80% MeOH−H_2O to yield **1** (1.11 mg), and C15 (163 mg) afforded **8** (1.98 mg) and **4** (0.79 mg) in the same procedure. Fractions C16 (50.4 mg) and C18 (96.5 mg) were purified by HPLC (COSMOSIL 5C_{18}-MS-II, 20 × 250 mm) with 75% MeCN−H_2O to yield **10** (1.14 mg) and **11** (0.64 mg), respectively. Fraction C17 (31.9 mg) was subjected to HPLC (InertSustain Phenylhexyl, 20 × 250 mm) with 85% MeOH−H_2O to yield **16** (5.60 mg). Fraction B10 (747 mg) was subjected to MPLC (SNAP Ultra C18, 12 g, Biotage Japan Ltd.) with a gradient system (70−100% MeOH–H_2O) to give 14 fractions (D1−D14). Fraction D8 (216 mg) was subjected to HPLC (InertSustain Phenylhexyl, 20 × 250 mm) with 70% MeOH−H_2O to yield 19 fractions (E1−E19). Fractions E6 (4.57 mg), E7 (13.4 mg), E8 (7.49 mg), and E15 (2.14 mg) were separately purified by HPLC (InertSustain Phenylhexyl, 20 × 250 mm) with 60% MeOH−H_2O to yield **5** (0.74 mg), **6** (1.10 mg), **2** (3.40 mg), and **9** (0.25 mg), respectively. Fractions E9 (18.5 mg), E10 (19.7 mg), and E14 (4.56 mg) were separately purified by HPLC (COSMOSIL 5C_{18}-MS-II, 20 × 250 mm) with 60% MeOH−H_2O to yield **3** (0.78 mg), **12** (1.32 mg), **15** (0.56 mg), and **14** (1.41 mg), respectively.

*Stellejasmins A (**1**):* White powder; $[\alpha]^{25}_{D}$ +21 (*c* 0.90, MeOH); UV (MeCN) λ_{max} (log ε): 272 (3.05), 230 (4.03), 196 (4.53) nm; IR (film) ν_{max} 3412, 3150, 3050, 2961, 2928, 2857, 2299, 2163, 1982, 1753, 1718, 1649, 1603, 1586, 1451, 1410, 1382, 1300, 1272, 1256, 1176, 1105, 1069, 1027, 1000, 985, 957, 935, 912, 839, 713 cm^{-1}; ^{1}H and ^{13}C NMR data ($CDCl_3$ and pyridine-d_5), Tables S1 and S3, respectively; HRTOFMS *m*/*z* 705.3038 $[M + H]^+$ (calcd for $C_{37}H_{50}ClO_{11}$, 705.3036).

*Stellejasmins B (**2**):* White powder; $[\alpha]^{25}_{D}$ +17 (*c* 2.8, MeOH); UV (MeCN) λ_{max} (log ε): 272 (2.87), 228 (4.00), 196 (4.51) nm; IR (film) ν_{max} 3419, 2964, 2925, 2856, 2164, 1980, 1750, 1717, 1647, 1603, 1584, 1451, 1382, 1315, 1271, 1231, 1177, 1141, 1129, 1108, 1078, 1071, 1026, 998, 993, 955, 946, 912, 808, 774, 756, 714, 612 cm^{-1}; ^{1}H and ^{13}C NMR data ($CDCl_3$), Table S2; HRTOFMS *m*/*z* 667.3129 $[M - H]^-$ (calcd for $C_{37}H_{47}O_{11}$, 667.3118).

*12-O-Benzoylphorbol 13-heptanoate (**3**):* White powder; $[\alpha]^{25}_{D}$ +14 (*c* 0.70, MeOH); UV (MeCN) λ_{max} (log ε): 228 (3.07), 196 (3.47) nm; IR (film) ν_{max} 3405, 2930, 2871, 2861, 2300, 2163, 1982, 1716, 1628, 1602, 1585, 1451, 1377, 1318, 1295, 1271, 1176, 1099, 1070, 1027, 1000, 969, 935, 902, 869, 805, 712 cm^{-1}; ^{1}H and ^{13}C NMR data ($CDCl_3$), Table S5; HRTOFMS *m*/*z* 603.2925 $[M + Na]^+$ (calcd for $C_{34}H_{44}NaO_8$, 603.2934).

Dry stem bark (1.8 kg) of *W. retusa* was extracted with MeOH. The extract (195 g) was partitioned between EtOAc and H_2O. The EtOAc−soluble fraction (70 g) was partitioned between *n*-hexane and 90% MeOH−H_2O. The 90% MeOH−H_2O fraction (56 g) was subjected to SiO_2 column chromatography with *n*-hexane, *n*-hexane−EtOAc, EtOAc, and MeOH to give 12 fractions (Frs. F1−F12). Fraction F7 (842 mg) eluted with 50% *n*-hexane−EtOAc (1:1) was subjected to MPLC (Purif-Pack-EX ODS 25 μm, 30 g, SHOKO SCIENCE Co., Ltd, Japan) with a gradient system using 20−100% MeOH-H_2O to yield 13 fractions. The eighth fraction was purified by HPLC (COSMOSIL 5C_{18}-MS-II, 20 × 250 mm) with 23, 35, 50, and 100% MeCN−H_2O to yield **18** (8.3 mg), **19** (1.6 mg), and **20** (13.4 mg).

Synthesis of Stelleracin A (13). Phorbol (26.3 mg, 0.072 mmol) was dissolved in anhydrous pyridine (0.5 mL) at 0 °C, and trityl chloride (101 mg, 0.36 mmol, 5 eq.) was

added to the solution under an argon atmosphere. The reaction mixture was stirred for 20 h at room temperature in the dark. The reaction was quenched with brine (5 mL) and extracted with CH_2Cl_2 (3 × 15 mL). The combined organic layer was washed with brine (10 mL) and dried over anhydrous Na_2SO_4. After filtration through a cotton pad and concentration under decreased pressure, the obtained crude residue was purified by column chromatography using CH_2Cl_2−MeOH (97:3 and 95:5) to afford 20-*O*-trityl phorbol (**IM-1**) (43.8 mg, 85% yield). The ^{1}H NMR data of **IM-1** was identical to reported data.[37] To a solution of **IM-1** (23.9 mg, 0.039 mmol) in anhydrous CH_2Cl_2 (1.5 mL), a CH_2Cl_2 solution of (4*Z*)-decenoic acid (0.17 M, 0.25 mL, 0.043 mmol, 1.1 eq.) was added at room temperature under an argon atmosphere. The mixture was then cooled at 0 °C, followed by addition of a solution of triethylamine (0.79 M, 0.1 mL, 0.079 mmol, 2.0 eq.), 1-ethyl-3-(3-dimethylaminopropyl)carbodiimide (EDC, 9.8 mg, 0.051 mmol, 1.3 eq.), and 4-(dimethylamino)pyridine (DMAP, 1.2 mg, 0.01 mmol, 20 mol %). After stirring for 14 h at room temperature in the dark, the reaction was quenched with brine (5 mL) and the aqueous layer was extracted with CH_2Cl_2 (3 × 15 mL). The combined organic layer was dried over anhydrous Na_2SO_4 and concentrated *in vacuo*. The crude residue was purified by column chromatography using 97 and 95% CH_2Cl_2−MeOH to afford 13-*O*-(4*Z*)-decenoyl 20-*O*-trityl phorbol (**IM-2**) (21.8 mg, 73% yield). **[Only simple separation and purification were carried out because intermediates IM-2 and IM-3 were unstable in light.]** To a solution of benzoic acid (42.5 mg, 0.34 mmol) in anhydrous CH_2Cl_2 (0.67 mL), a CH_2Cl_2 solution of triethylamine (2.3 M, 0.23 mL, 0.51 mmol, 1.5 eq.) and a CH_2Cl_2 solution of pivaloyl chloride (3.4 M, 0.1 mL, 0.34 mmol, 1.0 eq.) were successively added at 0 °C. The mixture was stirred at the same temperature for 1 h to obtain benzoic pivalic anhydride solution. To a solution of **IM-2** (20.2 mg, 0.028 mmol)

in anhydrous CH_2Cl_2 (0.9 mL), a CH_2Cl_2 solution of triethylamine (0.32 M, 0.1 mL, 0.032 mmol, 8 eq.), the above solution of benzoic pivalic anhydride (0.34 M, 0.7 mL, 0.24 mmol, 8 eq.), and DMAP (14.5 mg, 0.12 mmol, 4 eq.) were successively added at room temperature under an argon atmosphere. The reaction mixture was stirred for 24 h in the dark, and then the reaction was quenched with saturated $NaHCO_3$ solution (5 mL) and extracted with CH_2Cl_2 (3 × 15 mL). The combined organic layer was washed with brine (10 mL), dried over anhydrous Na_2SO_4, and concentrated *in vacuo*. The crude residue was quickly purified by column chromatography using 90% *n*-hexane−EtOAc to afford 12-*O*-benzoyl 13-*O*-(4*Z*)-decenoyl 20-*O*-trityl phorbol (**IM-3**) (15.2 mg, 62% yield). **IM-3** (15.1 mg, 0.018 mmol) was stirred together with 70% $HClO_4$ (3 μL, 2 eq.) in MeOH (1 mL) at room temperature in the dark for 12 h. To the reaction mixture, $NaHCO_3$ (1.0 mg) was added and stirred for 1 h. After evaporation of the solvent, the obtained residue was dissolved in water (5 mL) and extracted with EtOAc (3 × 15 mL). The combined organic layer was washed with brine (10 mL), dried over anhydrous Na_2SO_4, and concentrated *in vacuo*. The crude residue was purified by column chromatography using 50% *n*-hexane−EtOAc to afford **13** (8.6 mg, 0.014 mmol, 31% yield for 4 steps).

*Synthetic Stelleracin A (**13**):* White powder; UV (MeCN) λ_{max} (log ε): 274 (3.35), 234 (4.00) nm; IR (film) ν_{max} 3410, 2957, 2924, 2857, 1719, 1452, 1377, 1327, 1270, 1101, 969, 709 cm^{-1}; ^1H NMR ($CDCl_3$, 600 MHz) δ 8.03 (2H, dd, J = 7.5, 1.3 Hz), 7.62 (1H, br s), 7.57 (1H, tt, J = 7.5, 1.3 Hz), 7.45 (2H, t, J = 7.5 Hz), 5.75 (1H, s), 5.72 (1H, d, J = 5.0 Hz), 5.67 (1H, d, J = 10.2 Hz), 5.42 (1H, dt, J = 10.6, 7.2 Hz), 5.33 (1H,m), 4.07 (1H, d, J = 12.9 Hz), 4.02 (1H, d, J = 12.9 Hz), 3.34 (1H, m), 3.30 (1H, m), 2.60 (1H, d, J = 19.1 Hz), 2.51 (1H, d, J = 19.1 Hz), 2.45 (2H, m), 2.38 (2H, m), 2.33 (1H, m), 2.04 (2H, dd, J = 14.2, 7.1 Hz), 1.77 (3H, br s), 1.38 (3H, s), 1.36−1.23 (6H, m), 1.21 (3H, s), 1.14

(1H, d, J = 5.0 Hz), 0.95 (3H, d, J = 6.3 Hz), 0.88 (3H, t, J = 6.7 Hz); ^{13}C NMR ($CDCl_3$, 150 MHz) δ 209.0, 176.0, 166.2, 160.8, 140.5, 133.0, 132.9, 131.8 130.2, 129.7, 129.2, 128.5, 127.0, 78.3, 77.7, 73.7, 68.1, 65.6, 56.2, 43.3, 39.2, 38.7, 36.7, 34.5, 31.5, 29.2, 27.2, 26.0, 23.8, 22.5, 22.5, 17.0, 14.5, 14.0, 10.1; HRTOFMS m/z 643.3237 $[M + Na]^+$ (calcd for $C_{37}H_{48}NaO_8$, 643.3241).

General Procedure for the Preparation of 12,13-Diacylphorbols (21−28). These compounds were prepared following the procedure for **13**.

*12-O-(4Z)-Decenoylphorbol 13-Benzoate (**21**).* Compound **21** was prepared from phorbol (0.050 mmol), benzoic acid (0.064 mmol), and (4*Z*)-decenoic acid (0.160 mmol) (15.0 mg, 0.024 mmol, 43% yield over 4 steps). **21**: White powder; UV (MeCN) λ_{max} (log ε): 276 (3.27), 238 (4.07) nm; IR (film) ν_{max} 3414, 2957, 2928, 2878, 2857, 1740, 1699, 1452, 1377, 1324, 1283, 1158, 1122, 1073, 1027, 990, 984, 945, 908, 870, 713 cm^{-1}; ^{1}H NMR ($CDCl_3$, 500 MHz) δ 8.01 (2H, dd, J = 7.5, 1.3 Hz), 7.63 (1H, s), 7.58 (1H, tt, J = 7.5, 1.3 Hz), 7.44 (2H, t, J = 7.5 Hz), 5.94 (1H, s), 5.72 (1H, d, J = 5.0 Hz), 5.58 (1H, d, J = 10.2 Hz), 5.44 (1H, dt, J = 10.8, 7.3 Hz), 5.34 (1H, m), 4.06 (1H, d, J = 13.0 Hz), 4.01 (1H, d, J = 13.0 Hz), 3.30 (2H, m), 2.57 (1H, d, J = 19.2 Hz), 2.51 (1H, d, J = 19.2 Hz), 2.38 (4H, m), 2.21 (1H, m), 2.02 (2H, m), 1.80 (3H, dd, J = 2.9, 1.3 Hz), 1.34 (3H, s), 1.32 (3H, s), 1.27 (2H, m), 1.26 (2H, m), 1.25 (2H, m), 1.22 (1H, d, J = 5.0 Hz), 0.94 (3H, d, J = 6.5 Hz), 0.87 (3H, t, J = 7.0 Hz); ^{13}C NMR ($CDCl_3$, 125 MHz) δ 208.9, 172.8, 168.5, 160.8, 140.5, 133.7, 132.9, 132.8, 131.7, 129.9, 129.2, 128.5, 127.1, 78.2, 77.1, 73.7, 68.0, 66.0, 56.2, 43.2, 39.2, 38.7, 36.6, 34.6, 31.5, 29.2, 27.2, 26.4, 23.9, 23.0, 22.5, 16.9, 14.0, 14.5, 10.1; HRTOFMS m/z 643.3239 $[M + Na]^+$ (calcd for $C_{37}H_{48}NaO_8$, 643.3241).

*12-O-Benzoylphorbol 13-Propionate (**22**).* Compound **22** was prepared from phorbol (0.026 mmol), propionic acid (0.025 mmol), and benzoic acid (0.16 mmol) (8.6 mg, 0.016 mmol, 62% yield over 4 steps). **22**: White powder; UV (MeCN) λ_{max} (log ε): 266 (3.32), 234 (3.98) nm; IR (film) ν_{max} 3410, 2957, 2985, 2927, 2883, 1711, 1625, 1452, 1373, 1333, 1316, 1270, 1196, 1176, 1141, 1097, 1070, 1022, 977, 965, 935, 910, 882, 867, 807, 713 cm^{-1}; ^1H NMR ($CDCl_3$, 500 MHz) δ 8.03 (2H, dd, J = 7.5, 1.3 Hz), 7.61 (1H, br s), 7.57 (1H, tt, J = 7.5, 1.3 Hz), 7.45 (2H, t, J = 7.5 Hz), 5.78 (1H, s), 5.73 (1H, br d, J = 5.0 Hz), 5.66 (1H, d, J = 10.3 Hz), 4.06 (1H, d, J = 12.9 Hz), 4.01 (1H, d, J = 12.9 Hz), 3.34 (1H, t, J = 5.0 Hz), 3.29 (1H, m), 2.60 (1H, d, J = 19.0 Hz), 2.51 (1H, d, J = 19.0 Hz), 2.42 (1H, m), 2.38 (1H, m), 2.32 (1H, m), 1.76 (3H, dd, J = 2.8, 1.1 Hz), 1.38 (3H, s), 1.21 (3H, s), 1.17 (3H, t, J = 7.6 Hz), 1.14 (1H, d, J = 5.0 Hz), 0.95 (3H, d, J = 6.5 Hz); ^{13}C NMR ($CDCl_3$, 125 MHz) δ 209.0, 177.1, 166.3, 160.8, 140.5, 133.0, 132.9, 130.1, 129.7, 129.2, 128.4, 78.3, 77.7, 73.7, 68.1, 65.4, 56.2, 43.3, 39.1, 38.6, 36.6, 27.7, 26.0, 23.8, 17.0, 14.5, 10.1, 8.7; HRTOFMS m/z 547.2301 $[M + Na]^+$ (calcd for $C_{30}H_{36}NaO_8$, 547.2302).

*12-O-Benzoylphorbol 13-(4Z)-Decenoate (**23**).* Compound **23** was prepared from phorbol (0.033 mmol), (*E*)-decenoic acid (0.031 mmol), and benzoic acid (0.19 mmol) (8.3 mg, 0.013 mmol, 41% yield over 4 steps). **23**: White powder; UV (MeCN) λ_{max} (log ε): 264 (3.30), 234 (3.93) nm; IR (film) ν_{max} 3414, 2961, 2924, 2858, 1716, 1629, 1452, 1377, 1316, 1270, 1196, 1177, 1163, 1101, 1068, 1026, 980, 969, 935, 911, 867, 804, 709 cm^{-1}; ^1H NMR ($CDCl_3$, 500 MHz) δ 8.02 (2H, dd, J = 7.5, 1.0 Hz), 7.61 (1H, br s), 7.57 (1H, t, J = 7.5 Hz), 7.45 (2H, t, J = 7.5 Hz), 5.77 (1H, s), 5.71 (1H, br d, J = 5.0 Hz), 5.66 (1H, d, J = 10.2 Hz), 5.46 (1H, m), 5.39 (1H, m), 4.06 (1H, d, J = 12.8 Hz), 4.01 (1H, d, J = 12.8 Hz), 3.34 (1H, t, J = 5.0 Hz), 3.29 (1H, m), 2.61 (1H, d, J = 19.1 Hz), 2.51 (1H,

d, J = 19.1 Hz), 2.45 (1H, m), 2.41 (1H, m), 2.33 (1H, m), 2.31 (2H, m), 1.96 (2H, m), 1.76 (3H, br s), 1.38 (3H, s), 1.33−1.25 (6H, m), 1.21 (3H, s), 1.12 (1H, d, J = 5.0 Hz), 0.94 (3H, d, J = 6.4 Hz), 0.88 (3H, t, J = 7.7 Hz); ^{13}C NMR ($CDCl_3$, 125 MHz) δ 209.0, 176.0, 166.2, 160.8, 140.5, 133.0, 132.9, 132.0, 130.1, 129.7, 129.2, 128.4, 127.6, 78.3, 77.6, 73.7, 68.1, 65.5, 56.1, 43.3, 39.1, 38.6, 36.6, 34.4, 32.5, 31.4, 29.1, 27.5, 26.0, 23.8, 22.5, 17.0, 14.1, 14.5, 10.1; HRTOFMS m/z 643.3236 $[M + Na]^+$ (calcd for $C_{37}H_{48}NaO_8$, 643.3241).

*12-O-Benzoylphorbol 13-Stearate (**24**).* Compound **24** was prepared from phorbol (0.017 mmol), stearic acid (0.016 mmol), and benzoic acid (0.11 mmol) (8.8 mg, 0.012 mmol, 71% yield over 4 steps). **24**: White powder; UV (MeCN) λ_{max} (log ε): 262 (3.20), 232 (3.77) nm; IR (film) ν_{max} 3414, 3006, 2961, 2924, 2858, 1736, 1703, 1452, 1377, 1324, 1283, 1243, 1158, 1122, 1073, 1027, 994, 985, 946, 931, 907, 868, 713 cm^{-1}; ^{1}H NMR ($CDCl_3$, 500 MHz) δ 8.03 (2H, dd, J = 7.5, 1.0 Hz), 7.61 (1H, br s), 7.57 (1H, t, J = 7.5 Hz), 7.45 (2H, t, J = 7.5 Hz), 5.79 (1H, s), 5.73 (1H, br d, J = 5.0 Hz), 5.66 (1H, d, J = 10.3 Hz), 4.07 (1H, d, J = 12.9 Hz), 4.01 (1H, d, J = 12.9 Hz), 3.34 (1H, t, J = 5.0 Hz), 3.29 (1H, br s), 2.61 (1H, d, J = 19.2 Hz), 2.51 (1H, d, J = 19.2 Hz), 2.36 (2H, m), 2.33 (1H, m), 1.76 (3H, dd, J = 2.7, 1.0 Hz), 1.64 (2H, m), 1.38 (3H, s), 1.32−1.29 (28H, overlapped), 1.21 (3H, s), 1.13 (1H, d, J = 5.0 Hz), 0.94 (3H, d, J = 6.4 Hz), 0.87 (3H, t, J = 6.9 Hz); ^{13}C NMR ($CDCl_3$, 125 MHz) δ 209.0, 176.5, 166.1, 160.8, 140.5, 133.0, 132.9, 130.1, 129.7, 129.2, 128.4, 78.3, 77.7, 73.7, 68.1, 65.4, 56.2, 43.3, 39.1, 38.6, 36.7, 34.4, 29.7, 29.6, 29.4, 29.4, 29.2, 26.0, 24.6, 23.8, 22.7, 17.1, 14.5, 14.1, 10.1; HRTOFMS m/z 757.4649 $[M + Na]^+$ (calcd for $C_{45}H_{66}NaO_8$, 757.4650).

*12-O-Benzoylphorbol 13-Oleate (**25**).* Compound **25** was prepared from phorbol (0.023 mmol), oleic acid (0.021 mmol), and benzoic acid (0.13 mmol) (8.4 mg, 0.011

mmol, 51% yield over 4 steps). **25**: White powder; UV (MeCN) λ_{max} (log ε): 262 (3.18), 234 (3.75) nm; IR (film) ν_{max} 3410, 2965, 2924, 2858, 1723, 1376, 1327, 1270, 1191, 1177, 1141, 1104, 1097, 1055, 1013, 968, 934, 908, 804, 709 cm^{-1}; ^1H NMR ($CDCl_3$, 400 MHz) δ 8.02 (2H, dd, J = 7.5, 1.0 Hz), δ 7.61 (1H, br s), 7.57 (1H, t, J = 7.5 Hz), 7.45 (2H, t, J = 7.5 Hz), 5.80 (1H, s), 5.72 (1H, br d, J = 5.0 Hz), 5.66 (1H, d, J = 10.2 Hz), 5.34 (2H, m), 4.06 (1H, d, J = 12.7 Hz), 4.00 (1H, d, J = 12.7 Hz), 3.33 (1H, t, J = 5.0 Hz), 3.28 (1H, br s), 2.60 (1H, d, J = 19.0 Hz), 2.50 (1H, d, J = 19.0 Hz), 2.38 (2H, m), 2.33 (1H, m), 2.00 (4H, m), 1.76 (3H, br s), 1.63 (2H, m), 1.38 (3H, s), 1.34−1.23 (20H, overlapped), 1.20 (3H, s), 1.12 (1H, d, J = 5.0 Hz), 0.94 (3H, d, J = 6.4 Hz), 0.87 (3H, t, J = 6.6 Hz); ^{13}C NMR ($CDCl_3$, 100 MHz) δ 209.0, 176.5, 166.2, 160.8, 140.5, 133.0, 132.9, 130.1, 130.0, 129.8, 129.7, 129.2, 128.4, 78.3, 77.6, 73.7, 68.0, 65.4, 56.1, 43.3, 39.1, 38.6, 36.6, 34.4, 31.9, 29.8, 29.7, 29.5, 29.3, 29.3, 29.2, 29.1, 29.0, 27.2, 26.0, 24.5, 23.8, 22.7, 17.0, 14.5, 14.1, 10.1; HRTOFMS m/z 755.4493 $[M + Na]^+$ (calcd for $C_{45}H_{64}NaO_8$, 755.4493).

*12-O-Benzoylphorbol 13-Linoleate (**26**).* Compound **26** was prepared from phorbol (0.024 mmol), linoleic acid (0.023 mmol), and benzoic acid (0.15 mmol) (8.4 mg, 0.011 mmol, 46% yield over 4 steps). **26**: White powder; UV (MeCN) λ_{max} (log ε): 262 (3.26), 234 (3.84) nm; IR (film) ν_{max} 3414, 3010, 2957, 2928, 2854, 1716, 1456, 1373, 1332, 1270, 1184, 1177, 1139, 1101, 1071, 1069, 1057, 1008, 969, 935, 911, 867, 709 cm^{-1}; ^1H NMR ($CDCl_3$, 500 MHz) δ 8.03 (2H, dd, J = 7.5, 1.0 Hz), 7.61 (1H, br s), 7.57 (1H, t, J = 7.5 Hz), 7.45 (2H, t, J = 7.5 Hz), 5.78 (1H, s), 5.72 (1H, br d, J = 5.0 Hz), 5.66 (1H, d, J = 10.2 Hz), 5.25-5.41 (4H, m), 4.07 (1H, d, J = 12.9 Hz), 4.01 (1H, d, J = 12.9 Hz), 3.34 (1H, t, J = 5.0 Hz), 3.28 (1H, br s), 2.61 (1H, d, J = 19.0 Hz), 2.51 (1H, d, J = 19.0 Hz), 2.39 (2H, m), 2.33 (1H, m), 2.04 (4H, m), 1.76 (3H, br s, 1.0 Hz), 1.64 (2H, m), 1.38

(3H, s), 1.36−1.23 (14H, overlapped), 1.21 (3H, s), 1.13 (1H, d, J = 5.0 Hz), 0.94 (3H, d, J = 6.3 Hz), 0.88 (3H, t, J = 6.8 Hz); ^{13}C NMR ($CDCl_3$, 125 MHz) δ 209.0, 176.5, 166.2, 160.8, 140.5, 133.0, 132.9, 130.1, 130.1, 130.2, 129.7, 129.2, 128.4, 128.0, 127.9, 78.3, 77.6, 73.7, 68.1, 65.4, 56.2, 43.3, 39.1, 38.6, 36.7, 34.4, 31.5, 29.6, 29.3, 29.2, 29.1, 29.1, 27.2, 26.0, 25.6, 24.5, 23.8, 22.6, 17.1, 14.5, 14.1, 10.1; HRTOFMS m/z 753.4328 $[M + Na]^+$ (calcd for $C_{45}H_{62}NaO_8$, 753.4337).

*12-O-Benzoylphorbol 13-α-Linolenate (**27**).* Compound **27** was prepared from phorbol (0.023 mmol), α-linolenic acid (0.022 mmol), and benzoic acid (0.13 mmol) (8.8 mg, 0.012 mmol, 52% yield over 4 steps). **27**: White powder; UV (MeCN) λ_{max} (log ε): 262 (3.26), 234 (3.85) nm; IR (film) ν_{max} 3410, 3006, 2957, 2956, 2928, 2858, 1716, 1452, 1377, 1328, 1269, 1179, 1176, 1139, 1097, 1068, 1033, 1024, 969, 935, 911, 864, 804, 709 cm^{-1}; ^{1}H NMR ($CDCl_3$, 500 MHz) δ 8.02 (2H, dd, J = 7.5, 1.0 Hz), 7.61 (1H, br s), 7.57 (1H, tt, J = 7.5, 1.2 Hz), 7.45 (2H, t, J = 7.5 Hz), 5.78 (1H, s), 5.72 (1H, br d, J = 5.0 Hz), 5.66 (1H, d, J = 10.3 Hz), 5.41-5.29 (4H, m), 4.07 (1H, d, J = 12.9 Hz), 4.01 (1H, d, J = 12.9 Hz), 3.33 (1H, t, J = 5.0 Hz), 3.29 (1H, br s), 2.81 (4H, m), 2.60 (1H, d, J = 19.1 Hz), 2.50 (1H, d, J = 19.1 Hz), 2.39 (2H, m), 2.33 (1H, m), 2.06 (2H, m), 2.05 (2H, m), 1.76 (3H, dd, 2.8, 1.1 Hz), 1.64 (2H, m), 1.38 (3H, s), 1.36−1.25 (8H, overlapped), 1.21 (3H, s), 1.13 (1H, d, J = 5.0 Hz), 0.97 (3H, t, J = 7.6 Hz), 0.94 (3H, d, J = 6.5 Hz); ^{13}C NMR ($CDCl_3$, 125 MHz) δ 209.0, 176.5, 166.2, 160.8, 140.5, 133.0, 132.9, 131.9, 130.3, 130.1, 129.7, 129.2, 128.4, 128.3, 128.2, 127.7, 127.1, 78.3, 77.6, 73.7, 68.1, 65.4, 56.2, 43.3, 39.1, 38.6, 36.7, 34.4, 29.6, 29.2, 29.1, 29.0, 27.2, 27.2, 26.0, 25.6, 25.5, 23.8, 20.5, 17.1, 14.5, 14.3, 10.1; HRTOFMS m/z 751.4177 $[M + Na]^+$ (calcd for $C_{45}H_{60}NaO_8$, 751.4180).

*12-O-Benzoylphorbol 13-γ-Linolenate (**28**).* Compound **28** was prepared from phorbol (0.023 mmol), γ-linolenic acid (0.022 mmol), and benzoic acid (0.13 mmol) (6.6 mg, 0.009 mmol, 38% yield over 4 steps). **28**: White powder; UV (MeCN) λ_{max} (log ε): 262 (3.14), 234 (3.72) nm; IR (film) ν_{max} 3410, 3010, 2952, 2924, 2862, 1716, 1452, 1373, 1332, 1270, 1177, 1141, 1092, 1068, 1033, 1013, 964, 935, 911, 867, 709 cm^{-1}; ^1H NMR ($CDCl_3$, 500 MHz) δ 8.02 (2H, dd, J = 7.5, 1.0 Hz), 7.61 (1H, br s), 7.57 (1H, t, J = 7.5 Hz), 7.45 (2H, t, J = 7.5 Hz), 5.77 (1H, s), 5.72 (1H, br d, J = 5.0 Hz), 5.66 (1H, d, J = 10.3 Hz), 5.42-5.30 (6H, m), 4.07(1H, d, J = 12.9 Hz), 4.01 (1H, d, J = 12.9 Hz), 3.34 (1H, t, J = 5.0 Hz), 3.29 (1H, br s), 2.80 (4H, t, J = 5.1 Hz), 2.61 (1H, d, J = 19.2 Hz), 2.51 (1H, d, J = 19.1 Hz), 2.40 (2H, m), 2.33 (1H, m), 2.09 (2H, dd, J = 13.9, 7.1 Hz), 2.05 (2H, dd, J = 14.3, 7.4 Hz), 1.76 (3H, dd, J = 2.7, 1.0 Hz), 1.67 (2H, m), 1.45−1.23 (8H, overlapped), 1.38 (3H, s), 1.21 (3H, s), 1.13 (1H, d, J = 5.0 Hz), 0.94 (3H, d, J = 6.5 Hz), 0.88 (3H, t, J = 6.9 Hz); ^{13}C NMR ($CDCl_3$, 125 MHz) δ 209.0, 176.3, 166.2, 160.8, 140.5, 133.0, 132.9, 130.4, 130.1, 129.7, 129.6, 129.2, 128.4, 128.4, 128.2, 128.1, 127.6, 78.3, 77.6, 73.7, 68.1, 65.5, 56.2, 43.3, 39.1, 38.6, 36.7, 34.4, 31.5, 29.3, 29.0, 26.8, 26.0, 25.6, 24.1, 23.9, 22.6, 17.0, 14.5, 14.1, 10.1; HRTOFMS m/z 751.4177 $[M + Na]^+$ (calcd for $C_{45}H_{60}NaO_8$, 751.4180).

HIV-1 LTR-driven Transcriptional Activity Assay. TZM-bl cells were integrated with reporter genes for firefly luciferase and *Escherichia coli β*-galactosidase under the control of the long terminal repeat of HIV-1. TZM-bl cells (1×10^4 cells) were incubated with different concentrations of each compound for 24 h, and the HIV-1 LTR-driven transcriptional activity was determined by measuring the luciferase activity in the cell lysates. The EC_{50} values were calculated using GraphPad PRISM software (version 9) for a nonlinear regression with the maximum response of each compound as 100%.

Molecular Docking Simulations. Molecular modeling and docking simulations were performed using MOE.[38] A structure of the ligand-binding site of human PKC*β* was generated using the structure of mouse PKC*δ* in complex with phorbol 13-acetate (PDB ID: 1PTR) as a template. Comparison of the amino acid sequences of the ligand-binding sites between mouse PKC*δ* and human PKC*β* (yellow-colored in Figure S85a) revealed that Met239 and Trp252 in mouse PKC*δ*, and Ser110 and Tyr123 in human PKC*β* are not conserved (Figure S85a). The structure of the ligand-binding site of human PKC*β* was modeled by mutations of Met239 to Ser110 and of Trp252 to Tyr123 with the mouse PKC*δ* structure (Figure S85b). Hydrogen atoms were added to the modeled structure using the Protonate 3D module[39] and the structure was subjected to energy minimization using the Amber10:EHT force field. The energy minimization was performed with the hydrogen atoms and all the atoms of Ser110 and Tyr123. The resulting model of human PKC*β* was used for molecular docking simulations of the four compounds (**2**, **4**, **8**, and **10**). Their simplified models **2a**, **4a**, **8a**, and **10a** (Figure 7a) were docked at the ligand-binding site of the modeled human PKC*β* structure.[32] All molecular graphics were prepared using The PyMOL Molecular Graphics System (version 2.0, Schrödinger, LLC).

ASSOCIATED CONTENT

Supporting Information

The Supporting Information is available free of charge on the ACS Publications website.

^{1}H, ^{13}C, and 2D NMR spectra of new compounds **1**−**3**; ^{1}H NMR spectra of known compounds **4**−**20** and synthetic compound **13**; ^{1}H and ^{13}C NMR spectra of synthetic compounds **21**−**28**; NMR data (Tables) of **1**−**3**; PKC for molecular docking simulations (PDF)

Molecular formula strings of **1**−**20** with biological data; Molecular formula strings of synthetic compounds **21**−**28** and **13** with biological data (CSV)

Homology (docking) models (PDB)

ACKNOWLEDGMENT

This work was supported by JSPS KAKENHI Grants JP20K22710 (A.H.H.E.-D.), and JP20K16027 (K.E.), and JP19K07135 (T.K.), and Useful and Unique Natural Products for Drug Discovery and Development (UpRod), Program for Building Regional Innovation Ecosystems at Kumamoto University, Japan.

ABBREVIATIONS

AIDS, acquired immunodeficiency syndrome; ART, antiretroviral therapy; COSY, correlation spectroscopy; ECD, electronic circular dichroism; HIV, human immunodeficiency virus; HMBC, heteronuclear multiple bond correlation; HPLC, high-performance liquid chromatography; HRTOFMS, high-resolution time-of-flight mass spectrometry; IR, infrared; LRA, latency-reversing agent; MOE, Molecular Operating Environment; MPLC, medium pressure liquid chromatography; NMR, nuclear magnetic resonance; NOESY, nuclear Overhauser effect spectroscopy; ODS, octadecylsilane; PKC, protein kinase C; SAR, structure−activity relationship; TOCSY, total correlation spectroscopy; UV, ultraviolet; WHO, World Health Organization

REFERENCES

(1) *Summary of the global HIV epidemic, 2020.* https://www.who.int/data/gho/data/themes/hiv-aids (accessed October 28, 2021).

(2) Finzi, D.; Hermankova, M.; Pierson, T.; Carruth, L. M.; Buck, C.; Chaisson, R. E.; Quinn, T. C.; Chadwick, K.; Margolick, J.; Brookmeyer, R.; Gallant, J.; Markowitz, M.; Ho, D. D.; Richman, D. D.; Siliciano, R. F. Identification of a reservoir for HIV-1 in patients on highly active antiretroviral therapy. *Science* **1997**, *278*, 1295−1300.

(3) Wong, J. K.; Hezareh, M.; Guünthard, H. F.; Havlir, D. V.; Ignacio, C. C.; Spina, C. A.; Richma, D. D. Recovery of replication-competent HIV despite prolonged suppression of plasma viremia. *Science* **1997**, *278*, 1291−1295.

(4) Siliciano, J. D.; Kajdas, J.; Finzi, D.; Quinn, T. C.; Chadwick, K.; Margolick, J. B.; Kovacs, C.; Gange, S. J.; Siliciano, R. F. Long-term follow-up studies confirm the stability of the latent reservoir for HIV-1 in resting CD^{4+} T cells. *Nat. Med.* **2003**, *9*, 727−728.

(5) Chun, T. W.; Davey, R. T.; Jr., Engel, D.; Lane, H. C.; Fauci, A. S. Re-emergence of HIV after stopping therapy. *Nature* **1999**, *401*, 874−875.

(6) Chun, T.-W.; Carruth, L.; Finzi, D.; Shen, X.; DiGuiseppe, J. A.; Taylor, H.; Hermankova, M.; Chadwick, K.; Margolick, J.; Quinn, T. C.; Kuo, Y.-H.; Brookmeyer, R.; Zeiger, M. A.; Barditch-Crovo, P.; Siliciano, R. F. Quantification of latent tissue reservoirs and total body viral load in HIV-1 infection. *Nature* **1997**, *387*, 183−188.

(7) Andersen, R. J.; Ntie-Kang, F.; Tietjen, I. Natural product-derived compounds in HIV suppression, remission, and eradication strategies. *Antivir. Res.* **2018**, *158*, 63−77.

(8) Cashmore, A. R.; Seelye, R. N.; Cain, B. F.; Mack, H.; Schmidt, R.; Hecker, E. The structure of prostratin: a toxic tetracyclic diterpene ester from *Pimelea prostrata*. *Tetrahedron Lett.* **1976**, *17*, 1737−1738.

(9) Wender, P. A.; Kee, J.-M.; Warrington, J. M. Practical synthesis of prostratin, DPP, and their analogs, adjuvant leads against latent HIV. *Science* **2008**, *320*, 649−652.

(10) Sloanea, J. L.; Bennera, N. L.; Keenana, K. N.; Zanga, X.; Soliman, M. S. A.; Wu, X.; Dimapasoc, M.; Chun, T.-W.; Marsden, M. D.; Zack, J. A.; Wender, P. A.; Prodrugs of PKC modulators show enhanced HIV latency reversal and an expanded therapeutic window. *Proc. Natl. Acad. Sci. U.S.A.* **2020**, *117*, 10688−10698.

(11) Kupchan, S. M.; Shizuri, Y.; Murae, T.; Sweeny, J. G.; Haynes, H. R.; Shen, M.-S.; Barrick, J. C.; Bryan, R. F.; Helm, D. V. D.; Wu, K. K. Gnidimacrin and gnidimacrin 20-palmitate, novel macrocyclic antileukemic diterpenoid esters from *Gnidia subcordata*. *J. Am. Chem. Soc.* **1976**, *98*, 5719−5720.

(12) Lai, W.; Huang, L.; Zhu, L..; Ferrari, G.; Chan, C.; Li, W.; Lee, K.-H.; Chen, C.-H. Gnidimacrin, a potent anti-HIV diterpene, can eliminate latent HIV-1 ex vivo by activation of protein kinase Cβ. *J. Med. Chem.* **2015**, *58*, 8638−8646.

(13) Huang, L.; Lai, W.-H.; Zhu, L.; Li, W.; Wei, L.; Lee, K.-H.; Xie, L.; Chen, C.-H. Elimination of HIV-1 latently infected cells by gnidimacrin and a selective HDAC inhibitor. *ACS Med. Chem. Lett.* **2018**, *9*, 268−273.

(14) Liu, Q.; Cheng, Y.-Y.; Li, W.; Huang, L.; Asada, Y.; Hsieh, M.-T.; Morris-Natschke, S. L.; Chen, C.-H.; Koike, K.; Lee, K.-H. Synthesis and structure−activity relationship correlations of gnidimacrin derivatives as potent HIV-1 inhibitors and HIV latency reversing agents. *J. Med. Chem.* **2019**, *62*, 6958−6971.

(15) Abe, F.; Iwase, Y.; Yamauchi, T.; Kinjo, K.; Yaga, S. Daphnane diterpenoids from the bark of *Wikstroemia retusa*. *Phytochemistry* **1997**, *44*, 643−647.

(16) Abe, F.; Iwase, Y.; Yamauchi, T.; Kinjo, K.; Yaga, S.; Ishii, M.; Iwahana, M. Minor daphnane-type diterpenoids from *Wikstroemia retusa*. *Phytochemistry* **1998**, *47*, 833−837.

(17) Li, S.-F.; Liang, X.; Wu, X.-K.; Gao, X.; Zhang, L.-W. Discovering the mechanisms of wikstroelide E as a potential HIV-latency-reversing agent by transcriptome profiling. *J. Nat. Prod.* **2021**, *84*, 1022−1033.

(18) Tostes, J. B. F.; Carvalho, Andressa, L. D.; da Silva, A. J. R.; Mourão, P. J. P.; Rossi, A. D.; Tanuri, A.; Siani, A. C. Phorbol Esters from the Latex of *Euphorbia umbellata*: Bioguided Isolation of Highly Potent HIV-1 Latency Interrupters in Virus Reservoir Cells. *J. Nat. Prod*. **2021**, *84*, 1666−1670.

(19) Asada, Y.; Sukemori, A.; Watanabe, T.; Malla, K. J.; Yoshikawa, T.; Li, W.; Koike, K.; Chen, C.-H.; Akiyama, T.; Qian, K.; Nakagawa-Goto, K.; Morris-Natschke, S. L.; Lee, K.-H. Stelleralides A−C, novel potent anti-HIV daphnane-type diterpenoids from *Stellera chamaejasme* L. *Org. Lett.* **2011**, *13*, 2904−2907.

(20) Yan, M.; Lu, Y.; Chen, C.-H.; Zhao, Y.; Lee, K.-H.; Chen, D.-F. Stelleralides D−J and anti-HIV daphnane diterpenes from *Stellera chamaejas*. *J. Nat. Prod.* **2015**, *78*, 2712−2718.

(21) Hayes, P. Y.; Chow, S.; Somerville, M. J.; Voss, J. J. D.; Fletcher, M. T. Pimelotides A and B, diterpenoid ketal-lactone orthoesters with an unprecedented skeleton from *Pimelea elongate. J. Nat. Prod.* **2009**, *72*, 2081−2083.

(22) Pettit, G. R.; Zou, J.-C.; Goswami, A.; Cragg, G. M.; Schmidt, J. M. Antineoplastic agents, 88. *Pimelea prostrata*. *J. Nat. Prod.* **1983**, *46*, 563−568.

(23) Zayed, S.; Hafez, A.; Adolf, W.; Hecker, E. New tigliane and daphnane derivatives from *Pimelea prostrata* and *Pimelea simplex*. *Experientia* **1977**, *33*, 1554−1555.

(24) Asada, Y.; Sukemori, A.; Watanabe, T.; Malla, K. J.; Yoshikawa, T.; Li, W.; Kuang, X.; Koike, K.; Chen, C.-H.; Akiyama, T.; Qian, K.; Nakagawa-Goto, K.; Morris-Natschke, S. L.; Lu, Y.; Lee, K.-H. Isolation, structure determination, and anti-HIV evaluation of tigliane-type diterpenes and biflavonoid from *Stellera chamaejasme*. *J. Nat. Prod.* **2013**, *76*, 852−857.

(25) Dagang, W.; Sorg, B.; Adolf, W.; Opferkuch, H. J.; Seip, E. H.; Hecker, E. Oligo- and macrocyclic diterpenes in thymelaeaceae and euphorbiaceae occurring and utilized in yunnan (Southwest China). 4. Tigliane type diterpene esters (phorbol-12,13-diesters) from *Wikstroemia canescens*. *Phytother. Res.* **1993**, *7*, 194−196.

(26) Jiang, H.-Z.; Ma, Q.-Y.; Huang, S.-Z.; Liang, W.-J.; Wang, P.-C.; Zhao, Y.-X. A New tigliane-type diterpene ester from *Wikstroemia scytophylla*. *Chem. Nat. Compd.* **2012**, *48*, 587−590.

(27) Liang, S.; Shen, Y-H.; Feng, Yi; Tian, J-M.; Liu, X-H.; Xiong, Z.; Zhang, W-D. Terpenoids from *Daphne aurantiaca* and their potential anti-inflammatory activity. *J. Nat. Prod.* **2010**, *7*3, 532−535.

(28) Endo, Y.; Maruno, M.; Miura, N.; Baba, M.; Ikekawa, T. New diterpenes and antivirus agent containing diterpenes as active ingredient. Japan Patent JPH10287617A, October 20, 1998.

(29) Borris, R.; Cordell, G. A. Studies of the thymelaseceae II. Antineoplastic principles of *Gnidia kraussiana*. *J. Nat. Prod.* **1984**, *47*, 270−278.

(30) Hayes, P. Y.; Chow, S.; Somerville, M. J.; Fletcher, M. T.; Voss, J. J. D. Daphnane- and tigliane-type diterpenoid esters and orthoesters from *Pimelea elongate*. *J. Nat. Prod.* **2010**, *73*, 1907−1913.

(31) Zhang, G.; Kazanietz, M. G.; Blumberg, P. M.; Hurley, J. H. Crystal structure of the cys2 activator-binding domain of protein kinase Cδ in complex with phorbol ester. *Cell* **1995**, *81*, 917−924.

(32) Corbeil, C. R.; Williams, C. I.; Labute, P. Variability in docking success rates due to dataset preparation. *J. Comput. Aided Mol. Des.* **2012**, *26*, 775−786.

(33) Allard, P.-M.; Leyssen, P.; Martin, M.-T.; Bourjot, M.; Dumontet, V.; Eydoux, C.; Guillemot, J.-C.; Canard, B.; Poullain, C.; Guéritte, F.; Litaudon, M. Trigocherrin A, the first natural chlorinated daphnane diterpene orthoester from *Trigonostemon cherrieri*. *Org. Lett.* **2012**, *14*, 342−345.

(34) Allard, P.-M.; Leyssen, P.; Martin, M.-T.; Bourjot, M.; Dumontet, V.; Eydoux, C.; Guillemot, J.-C.; Canard, B.; Poullain, C.; Guéritte, F.; Litaudon, M. Antiviral chlorinated daphnane diterpenoid orthoesters from the bark and wood of *Trigonostemon cherrieri*. *Phytochemistry* **2012**, *84*, 160−168.

(35) Newton, A. C. Protein kinase C: perfectly balanced. *Crit. Rev. Biochem. Mol. Biol.* **2018**, *53*, 208−230.

(36) Szallasi, Z.; Smith, C. B.; Blumberg, P. M. Dissociation of phorbol esters leads to immediate redistribution to the cytosol of protein kinases Cα and Cδ in mouse keratinocyte. *J. Biol. Chem.* **1994**, *269*, 27159−27162.

(37) Boudreault, P.-L.; Mattler, J. K.; Wender, P. A. Studies on the regio- and diastereo-selective epoxidation of daphnanes and tiglianes. *Tetrahedron Lett.* **2015**, *56*, 3423−3427.

(38) *Molecular Operating Environment (MOE)*, version 2020.09; Chemical Computing Group: Montreal, Quebec, Canada.

(39) Labute, P. Protonate3D: Assignment of ionization states and hydrogen coordinates to macromolecular structures. *Proteins* **2009**, *75*, 187−205.

Table of Contents graphic